

NASA Technical Paper 1421

Wind-Tunnel Investigation
of the Validity of a
Sonic-Boom-Minimization Concept

Robert J. Mack and Christine M. Darden

OCTOBER 1979

**CASE FILE
COPY**

NASA



NASA Technical Paper 1421

Wind-Tunnel Investigation
of the Validity of a
Sonic-Boom-Minimization Concept

Robert J. Mack and Christine M. Darden
Langley Research Center
Hampton, Virginia



National Aeronautics
and Space Administration

**Scientific and Technical
Information Branch**

1979

SUMMARY

A wind-tunnel investigation has been conducted to determine the validity and applicability of a sonic-boom-minimization theory. Five models - two reference and three low-boom constrained - were tested at design Mach numbers of 1.5 and 2.7 and at angles of attack which provided the same lift. Pressure signatures were measured at a distance of 3 low-boom body lengths and were compared with signatures computed from descriptions of model geometry. Sensitivity studies were performed on the low-boom models at angles of attack 20 percent above and below the design point at Mach numbers of 1.5, 2.6, 2.7, and 2.8.

Results showed that the pressure signatures generated by the low-boom models had significantly lower overpressure levels than those produced by the reference models. Mach number and angle-of-attack sensitivity of the low-boom-model pressure signatures were found to be small.

Boundary-layer effects were sizable on the low-boom models, and when viscous corrections were included in the analysis, improved agreement between the predicted and the measured signatures was noted. However, the agreement was better at Mach 1.5 than at Mach 2.7. It was concluded that the minimization theory was valid at Mach 1.5 and was probably valid at Mach 2.7, with further study needed to resolve the uncertainty.

INTRODUCTION

The first supersonic cruise aircraft were designed to fly at the highest possible aerodynamic efficiency with little concern given to the sonic boom these aircraft would generate. However, ground overpressures from aircraft in test flights at supersonic Mach numbers were found to be so high as to cause considerable public concern. As a result, legal prohibitions on the overland supersonic flight of commercial transports were passed. Clearly, low sonic boom would have to be an equally important consideration along with other factors in the design of future supersonic transport aircraft for there to be any hope of removing present restrictions.

An analytic method that would permit sonic-boom minimizing constraints to directly influence the overall aircraft design was derived by Seebass and George (ref. 1). The method provides a constraint on the aircraft equivalent-area distribution. Aircraft features can be shaped and components positioned within this area envelope so as to keep the ground overpressures at a predetermined level while maximum aerodynamic and structural efficiencies are being sought. A previous analytical study (ref. 2) showed that sonic-boom levels could be reduced considerably by judiciously applying these boom-minimization concepts. These favorable results indicated the need for experimental verification of the minimization method by a wind-tunnel test program involving models designed to match sonic-boom constraints.

Five wing-body models were used in this wind-tunnel study. There were two reference models - an unconstrained delta wing and an unconstrained arrow wing - and three models designed for low-boom performance - one Mach 1.5 low-boom arrow-wing and two Mach 2.7 low-boom arrow-wing models. The nonboom-constrained models were included to provide reference pressure signatures that could be compared with those produced by the minimum sonic-boom models.

Pressure signatures were measured at a distance of 45.72 cm (18.0 in.), which is 3 low-boom body lengths. Design Mach numbers were 1.5 and 2.7; additional tests were performed at Mach numbers of 2.6 and 2.8 and at angle-of-attack to design-angle-of-attack ratios of 0.8, 1.0, and 1.2 to determine the shape and overpressure sensitivity of the low-boom pressure signatures.

SYMBOLS

Because these wind-tunnel models were designed initially as full-size aircraft (with enlargements for sting support), certain parameters such as l_e , A_e , and x_e , have two characteristic sets of dimensions. When the full-scale aircraft is referred to, the dimensions are in meters (feet); when the model is referred to, the dimensions are in centimeters (inches).

A_e	effective area due to area-ruled volume and lift
$C_{L\alpha}$	theoretical lift-curve slope
D	model sting diameter
d	dihedral height
F	Whitham F-function
h	radial distance normal to wind vector from nose (see fig. 10)
Δh	incremental displacement of model nose due to lift (see fig. 9(a))
K_r	sonic-boom reflection factor
k	deflection per unit load of model nose, $\Delta\alpha/\Delta L$
ΔL	incremental lift load used to determine k (see fig. 9(b))
l	overall length of model or aircraft
l_e	effective length of model or aircraft
M	free-stream Mach number
p	free-stream static pressure, Pa (lbf/ft ²)

Δp	incremental pressure due to model flow field, Pa (lbf/ft ²)
q	wind-tunnel dynamic pressure, $\frac{\gamma}{2} \rho M^2$, Pa (lbf/ft ²)
S	wing area
W_C	aircraft weight at start of cruise, kg (lb)
x	longitudinal ordinate
Δx	incremental distance along pressure signature
x_e	effective distance along windward direction
y	spanwise coordinate
α	angle of attack, degrees and minutes
$\Delta\alpha$	change in α due to lift-induced sting deflection (see fig. 9)
β	$= \sqrt{M^2 - 1}$
γ	ratio of specific heats (1.4 for air)
δ_e^*	effective area due to estimated boundary-layer displacement thickness
ϵ	wind-tunnel flow angle along model travel, arc minutes
θ	angle setting on prism in angle-of-attack mechanism, degrees and minutes
λ	fraction of equivalent length for nose "spike" (see fig. 5)
μ	Mach angle, $\sin^{-1} \frac{1}{M}$

Subscripts:

D	design condition at cruise Mach number and altitude
f	fuselage
le	leading edge
w	wing

BACKGROUND

Current minimum-boom theory and design methods are due to the accumulated efforts of many researchers during the past quarter century. The basic sonic-boom theory originated in a classic paper (ref. 3) by G. B. Whitham. Whitham theory is a modification of linearized theory to account for the coalescence of disturbances into shocks for bodies of revolution. Basic to its application is the formulation of the F-function which relates the area distribution of the aircraft that is generating flow-field disturbances to an appropriate source distribution. The analysis of reference 4 showed that Whitham theory could also be applied to winged bodies. Since efficient supersonic cruise aircraft are, in general, slender small-disturbance bodies, Whitham theory has been useful in predicting sonic-boom overpressures.

Concurrently with theory-validating experimental programs such as those mentioned in reference 5, studies were conducted to define minimum-sonic-boom-generating bodies. The concept of the far-field lower bound was introduced in reference 6. For these lower-bound bodies, F-functions are simply delta-function pulses which give effective areas A_e proportional to $x_e^{1/2}$ (fig. 1) and which generate minimum-impulse, far-field, N-wave signatures. Aircraft represented by lower-bound effective areas are usually very blunt and have high drag characteristics.

A later analysis, reference 7, pointed out that because of the appreciable length of proposed supersonic cruise aircraft, near-field characteristics of the pressure signature could persist out to significant distances at Mach numbers up to $\sqrt{2}$. An experimental study which tested these concepts is described in reference 8. The good agreement between measured and predicted pressure signatures at $M = 2.0$ as well as $M = \sqrt{2}$ proved that the basic idea was sound.

Further progress in the development of sonic-boom theory came from the signature-propagation work of reference 9. In a report which described a computer program for extrapolating a pressure signature through a stratified atmosphere, it was shown that real atmosphere effects tended to "freeze" the signature shape well before the pressure disturbances reached the ground. This reinforced the earlier hypothesis that near-field shape features would be preserved during the transonic acceleration phase of flight and extended it to supersonic cruise conditions.

The far-field minimum-boom concept, the shape-persistence hypothesis, and the shape-freezing tendencies of the atmosphere were combined into the isothermal-atmosphere-boom-minimization theory of reference 1. A delta-function pulse was placed at the front of a flat-top F-function or at the front of a linearly increasing F-function in a manner that minimized the shock overpressure or the nose shock, respectively. Also, a provision for making the tail shock equal in strength to the nose shock was included. The work of references 10 and 11 extended the minimization theory of reference 1 to a standard atmosphere and replaced the delta-function pulse with a finite, triangular "spike." It was shown that this modification would produce a configuration with a lower drag and only a small increase in shock overpressure and impulse. In figure 1, a comparison of effective-area distributions computed from the minimum-impulse F-function of reference 6, the minimum-overpressure F-function

of reference 1, and the spiked F-function of reference 11 is shown to illustrate the development of minimization concepts. Only the positive part of the F-function, where the effects of the different area constraints are most evident, is shown in each case. Overpressures for each body, calculated at a typical cruise altitude, are also shown.

The curves are calculated for bodies of length l_e and a maximum effective area of $0.01l_e^2$. A peak-to-plateau ratio on the spiked F-function was 6.5, about the same value as on the F-functions of the models designed for minimum boom at $M = 2.7$. The flat-top F-function of reference 1 was calculated from the same propagation condition that was imposed on the spiked F-function; that is, on the ground the pulse and the "spike" would disappear.

The far-field, minimum-impulse F-function of reference 6 gives a high-drag body because of the rapid growth of equivalent area. Some drag reduction is possible on the body designed from the F-function of reference 1 along with a substantial reduction in overpressure. Further drag reductions are possible on the body which gives the spiked F-function of reference 11, but at the penalty of slightly higher overpressures than from the signature of reference 1. Since the spike width is variable, drag--sonic-boom trade-off studies are possible. In the present wind-tunnel study, $\lambda = 0.1$ was used in the calculation of minimum-boom-constraint curves for the low-boom models.

MODEL DESCRIPTION

The five models used in the study are shown in figure 2, where their plan-view features and relative size can be easily seen. Two models - the delta wing and the arrow wing - were the reference models, while the other three were designed to low-boom constraints. They are 1/600-scale copies of full-size aircraft. Inviscid-flow assumptions were used in designing the low-boom models to meet equivalent-area constraints. However, Reynolds numbers effects were included in the analysis of data by adding an incremental effective area due to displacement thickness which was computed from the method of reference 12.

Since basic sonic-boom minimization concepts were being tested, wing-body models were judged sufficient to demonstrate the effects of the volume and lift contributions. Aircraft components such as horizontal and vertical tails, engine nacelles, and wing fences were not included to simplify design and construction. For the same reasons, the models were designed with circular, uncambered fuselages and flat, planar wings having sharp leading and trailing edges.

Reference Models

An unconstrained delta-wing model which resembled an early supersonic cruise vehicle concept and an unconstrained arrow-wing model with features that emphasized high-aerodynamic-efficiency, supersonic cruise technology were used as standards for comparison of performance with the three models configured for low sonic boom. A three-view drawing of the delta-wing-body model is seen in figure 3(a) and that of the arrow-wing-body model in figure 3(b).

Low-Boom Models

The three low-boom models were obtained by designing aircraft according to the minimum sonic-boom area distributions obtained from the computer program of reference 11. Two aircraft were designed to cruise at $M = 2.7$ and an altitude of 18 288 m (60 000 ft) while the third was to cruise at $M = 1.5$ and an altitude of 15 240 m (50 000 ft). A Mach number of 2.7 was chosen because it was used in the early feasibility studies and is approaching the upper limits of near-field sonic-boom theory. A Mach number of 1.5 was judged to be near the lower limit for a supersonic cruise aircraft and is in the range where linearized theory is accepted as valid for slender bodies.

A schematic outline of the computerized sonic-boom minimization process which calculates the effective-area constraint curve, the F-function, and the ground pressure signature is shown in figure 4. The input parameters are listed as design conditions. Note that neither the minimum nose shock Δp nor the minimum overpressure Δp is among the input parameters. These pressures are a function of the design conditions and must be assessed by the designer as either excessive or satisfactory. If Δp is too large, one or more design conditions must be changed and the program recycled until an acceptable value is calculated.

For all three of the test low-boom models, the minimum overpressure (spiked, flat-top) option was chosen with an acceptable Δp from their full-scale counterpart to be approximately 50 Pa (1 lbf/ft²). The ratio of nose to tail shock of the pressure signatures was 1.0.

Although the minimization procedure provides an effective-area curve, the aircraft meeting this constraint can still reflect a variety of design approaches. This is illustrated in figure 5 for two Mach 2.7 low-boom wing-body configurations. Both aircraft meet the same design conditions, have the same "spike" flat-top F-function, and produce the same ground-level sonic-boom signature. The most noticeable differences are in the wing planforms and the effective-area distributions of the volume and the lift. Obviously there is no unique aircraft shape. Other configurations can be designed to meet the same cruise flight conditions and still produce the same minimum overpressure signature. This is due to the variety of ways that lift and volume can be combined to satisfy both sonic-boom constraints and aerodynamic, structural, etc. requirements.

The three low-boom aircraft were designed with a cruise weight of 272 155 kg (600 000 lb) and an equivalent length of 91.44 m (300 ft). In addition, the "spike" width ratio λ was chosen as 0.1, since this represented a first-cut trade-off between shock level and drag. This is the only drag consideration included in the study. A ground-reflection factor of 1.9 was used in the pressure-signature calculations.

Additional effective area was included to account for the effects of the model sting, which was sized to withstand the stresses to be imposed. Its effective area was then included in the minimization program so that the final effective-area constraint curve included sting effects.

Two aircraft were designed to match the minimum overpressure-equivalent-area curve defined from a Mach number of 2.7 and an altitude of 18 288 m (60 000 ft), and one aircraft was designed to match the constraint curve defined from a Mach number of 1.5 and an altitude of 15 240 m (50 000 ft). Of the two aircraft designed for $M = 2.7$, one used only volume to meet area requirements near the nose while the other - a blunt-apex arrow - used both volume and lift. Figures 2 and 5 illustrate the differences between these two Mach 2.7 aircraft.

The design process was iterative and began by making a first-cut wing-body design. This design was analyzed with the wave-drag area rule program (ref. 13) and a wing analysis program (ref. 14) which had been modified to calculate both volume and lift effective-area contributions. A comparison of the resulting equivalent-area curve and the constraint curve indicated where changes should be made to improve the agreement of the curves. This iteration process was continued until acceptable agreement was reached.

The features common to all the final designs are shown in figure 6 and were varied in the iteration process to match the effective areas. Wing camber and twist were not employed because of the small size of the models, but dihedral was used specifically to control effective length. The effect of dihedral on the effective length is shown in figure 7.

When a satisfactory solution was obtained, 1/600-scale wind-tunnel models were constructed from the designs. Three-view drawings of these designs are shown in figures 8(a), 8(b), and 8(c). Detailed descriptions (in wave-drag program format) of the full-size aircraft are given in table I.

TEST APPARATUS AND PROCEDURE

Model Deflection Measurements

Since the models were 1/600 scale (i.e., 15.24 cm (6.0 in.) or less in length), a small prism for measuring the model angle of attack was mounted in the sting support of the angle-of-attack mechanism. Attitude and position corrections were obtained from a measurement of model deflection and pitch-angle increments due to imposed static loads. Figure 9(a) shows a sketch of the undeflected and deflected model; figure 9(b), the deflection lines obtained with the models under load in the angle-of-attack mechanism. These lines were computed from a linear, least-squares fit of the measurement points. Note that corrections in both angle and displacement were recorded, the first for determining the correct prism angle and the second as an incremental correction to the distance between model and measuring probe.

Pressure-Measurement Apparatus

Figure 10 is a sketch of the model, model support system, and pressure rake used during the test. Model angle of attack is controlled by the angle-of-attack mechanism mounted on the model longitudinal motion actuator. Angle of attack is positive in rotation away from the pressure rake and is measured

with a wind-tunnel spectrometer from the prism set into the model sting-support arm of the angle-of-attack mechanism (fig. 9(a)).

The model is moved forward or aft during the measurement of the pressure signature by the model longitudinal actuator mounted on the wind-tunnel sidewall. Differential pressures were measured with a pressure rake having a measuring probe and a reference probe mounted in the offset position shown in figure 10. Each probe was a 2° half-angle cone with two orifices set 180° apart connected to a common chamber. The measuring probe was positioned in a plane which coincided with the model plane of symmetry in pitch. Its axis was parallel with the tunnel center line and the orifices were positioned 90° to the plane containing the probe axis and the model plane of symmetry.

The pressure probes and rake were mounted on the tunnel sting support, which provided positioning both longitudinally along the tunnel test section as well as laterally across the test section (i.e., toward and away from the model). Model and measuring probe positioning were remotely controlled during the test run from the control console.

Pressure Measurements

The wind-tunnel tests were conducted at a Mach number of 1.5 in the low-speed test section and at Mach numbers of 2.6, 2.7, and 2.8 in the high-speed test section of the Langley Unitary Plan wind tunnel. Constant values of Reynolds number, 6.56×10^6 per meter (2.0×10^6 per foot), and stagnation temperature, 338.7 K (150° F), were maintained at all Mach numbers. The stagnation pressures used were 53 195 Pa (1111 lb/ft^2), 85 675 Pa (1790 lb/ft^2), 90 397 Pa (1888 lb/ft^2), and 95 329 Pa (1991 lb/ft^2) at Mach numbers of 1.5, 2.6, 2.7, and 2.8, respectively.

Flow-angle surveys established incremental flow angles of 6.8 arc minutes and 6.0 arc minutes (angled away from the tunnel sidewall) for the respective Mach numbers of 1.5 and 2.7. Surveys were not made at Mach numbers of 2.6 and 2.8 because it was assumed that the ± 0.1 increment in Mach number would not change the flow angle significantly. These flow-angle increments were used to correct the prism-angle settings so that the models would be at the required angle of attack. (See fig. 9(a).)

Pressure signatures were measured at a distance (normal to the wind direction) of 45.72 cm (18 in.) from the model nose. The individual pressure signatures produced by the reference models and the Mach 2.7 low-boom arrow-wing models are shown in figures 11(a) to 11(d). In figures 11(e) and 11(f), these signatures have been overlaid to facilitate comparisons between the reference models and the two low-boom models. A similar arrangement of measured pressure signatures is seen in figures 12(a) to 12(d) for the reference models and the Mach 1.5 low-boom arrow-wing model. In both figures 11 and 12, the angles of attack are those calculated to produce a level-flight lift of 272 155 kg (600 000 lb) on the full-scale aircraft.

For the Mach 2.7 low-boom models, sensitivity studies were made for both angle of attack and Mach number. Sensitivity to angle of attack was investi-

gated at Mach numbers of 1.5 and 2.7 by measuring pressure signatures at angles which were 20 percent above and below the design angle of attack. (See table II.) Mach number sensitivity pressure signatures were measured at Mach numbers of 2.6 and 2.8 with the Mach 2.7 low-boom arrow-wing model set at design-lift angle of attack. Since stable supersonic flow could not be established at a Mach number of 1.4, the Mach number sensitivity tests were not made for the Mach 1.5 low-boom model.

In figures 13(a) and 13(b), the results of these angle-of-attack and Mach number sensitivity tests are shown for the Mach 2.7 low-boom arrow-wing model. Since the measured pressure signatures from the angle-of-attack sensitivity tests for the Mach 1.5 low-boom arrow-wing model and the Mach 2.7 low-boom, blunt-apex arrow-wing model showed the same trends, they were not included in this report.

RESULTS AND DISCUSSION

The measured pressure signatures of figures 11 to 13 show distinct differences which mark them as generated by either the reference models or by the low-boom models. In figure 11(a), the effects of rapid lift buildup and short lift development length are seen as a near-field N-wave. Figure 11(b) shows that a more gradual lift buildup coupled with a slightly longer lift development length gives a pressure signature in which both the nose and the lift-induced shocks are seen in the near field. Similar results were measured at $M = 1.5$ also, as seen in figures 12(a) and 12(b).

In contrast, the pressure signatures from the low-boom models (figs. 11(c), 11(d), and 12(c)) show the benefits of a gradual and constrained lift buildup, an appreciably extended lift development length, special nose blunting, etc. Definite near-field and flat-top characteristics are seen, although they are somewhat masked by unexpected ripples and overshadowed by a compression peak just before the final expansion. As will be shown, a significant amount of these departures from the desired pressure signatures can be attributed to sizeable viscous effects on the small wind-tunnel models. These effects were not included in the full-scale aircraft designs because they could not be properly scaled down to model size.

Signatures from the unconstrained models and each of the low-boom models are overlaid for easier comparisons in figures 11(e), 11(f), and 12(d). Considering only the forward part of the low-boom signatures, where viscous effects are small, these comparisons show the low-boom pressure levels to be about one-third those of the delta wing and about one-half those of the arrow wing - a significant reduction.

The relative sensitivity of signature shape and overpressure strength to off-design Mach number and angle of attack is seen in figure 13. A change of ± 0.1 in Mach number is barely noticeable on the pressure signatures in figure 13(a). The prominent differences between the three signatures in figure 13(b) reflect a 20-percent change in angle of attack. If the angle-of-attack increments were of the same proportionate size as the Mach number increments, very little difference in shape or overpressure strength would be

seen. These results indicate that shock strength and impulse levels in minimum-overpressure signatures are relatively insensitive to changes of 3 to 4 percent in Mach number and/or angle of attack.

In order to estimate the viscous effects on the wind-tunnel models, boundary-layer displacement thicknesses on the wing and body surfaces were calculated using the method of reference 12, and the incremental area contributions were added to the distributions of model effective area due to volume. These displacement-thickness-modified areas were used along with the original lift distributions to get a new set of corrected theoretical signatures.

In figures 14(a) to 14(c), effective-area distributions, a measured pressure signature, and three theoretical pressure signatures are shown and compared for each of the low-boom models at their respective design condition. The inviscid-theory signatures were calculated from the measurements of the constructed models; the theory (with viscous effects) signatures were calculated from the model measurements plus corrections for boundary-layer displacement thickness; and the inviscid, boom-constrained theory signatures were calculated from the low-boom F-function provided by the minimization program of reference 11.

These signature comparisons were made at a distance of 3 body lengths rather than at an extrapolated ground distance because the model boundary layer was not the same as, or necessarily similar to, the boundary layer on the full-scale aircraft. A discussion of signature extrapolation is presented after the comparison of signatures.

Since both the measured and the predicted signatures are near-field, some of the F-function "spike" is still seen at, and just aft of, the nose shock. This residual minimization feature disappears in the midfield and, on the ideal low-boom signature, leaves a plateau-shaped pressure wave.

The saw-tooth perturbations in the inviscid-theory signature, as compared with the inviscid boom-constrained theory signature, are due to the imperfect matching of the ideal and the model effective-area curves and to unavoidable, small, construction inaccuracies. These effects, plus those due to viscosity, appear in the viscous-corrected signatures; thus, none of the theoretical signatures are perfectly flat from nose shock to expansion point.

The agreement between theoretical and experimental signatures improves as the comparison signature changes from the inviscid, boom constrained to the inviscid and finally to the viscous corrected. Mach number effects are definitely present. At a Mach number of 1.5, the agreement between measured and predicted signatures is good from nose shock to tail shock; while at a Mach number of 2.7, the agreement is very good only from the nose shock to the compression peak just before the final expansion. The poor agreement on this aft section of the pressure signatures at $M = 2.7$ has been noted before at various Mach number and lift conditions such as those described in references 8, 15, and 16. Some of the wing and wing-body models in these references had

leading-edge sweep angles which changed, along the semispan, from subsonic to supersonic in character - as did the leading edges on the Mach 2.7 low-boom arrow-wing models. This type of leading edge might be producing the Δp increment between the measured and viscous-corrected signature levels which is seen on the preexpansion peaks in figures 14(a) and 14(b). It could also account for the changing character of this preexpansion peak that is seen in figure 13(b).

Thus, boundary-layer displacement-thickness correction accounts for most of the measured and inviscid theory signature differences at $M = 1.5$ and the major part of these differences at $M = 2.7$. However, possible inaccuracies in the prediction of the effective lift distribution, as well as the possibility that the limits of linearized theory are being approached, could be contributing to the poor agreement at the higher Mach number.

Since wind-tunnel-model pressure signatures are measured in the near field, estimates of ground overpressures are found by extrapolating theoretical signatures (based on model geometry) or measured signatures from a cruise altitude to the ground. In figure 15, both of these extrapolations are shown and compared at the test Mach numbers of 2.7 and 1.5. The ideal, boom-constrained signatures were provided by the minimization program; the viscous-flow model and inviscid-flow model theory signatures were calculated with the method of reference 9, while the extrapolated wind-tunnel signatures were obtained by using the method of reference 17.

Good agreement between the ideal and the model extrapolated signatures in the inviscid theory calculations is seen at both Mach numbers since this was the basis of the model design. Comparisons of extrapolated wind-tunnel and viscous theory signatures do not show a similar good agreement at $M = 2.7$ but do at $M = 1.5$. Since only boundary-layer displacement-thickness corrections were applied, the previous comments concerning the viscous-flow corrections in the near-field signature comparisons also apply in these extrapolated signature comparisons. Thus, the good results at $M = 1.5$ lead to the conclusion that at the lower supersonic Mach numbers, an aircraft designed such that its volume, lift, boundary layer, etc. are constrained by a minimization-theory effective-area curve will generate a ground-level signature almost identical to that predicted by theory. The limited agreement between theory and experiment at $M = 2.7$ suggests that the minimization theory is probably valid but that further study is needed to establish this as a firm conclusion.

CONCLUDING REMARKS

A wind-tunnel study was conducted with two reference models and three low-boom models which were designed with the Seebass and George sonic-boom minimization theory. The conclusion that the method was valid and applicable to the design of supersonic cruise aircraft was shown to be justified at the test Mach number of 1.5. Encouraging results were obtained at a Mach number of 2.7, but further work is needed to assess the theory up to this higher Mach number.

Pressure signatures from the low-boom models were found to be relatively insensitive to small differences in Mach number and lift conditions from the design point. Boundary-layer effects were found to be significant on the slender low-boom models which had appreciable wing areas and extended lift-development lengths. Corrections for these viscous effects significantly improved the agreement between the measured and the predicted signatures in the near field and between the extrapolated wind tunnel and the viscous corrected theory signature in the far field (cruise altitude condition).

Langley Research Center
National Aeronautics and Space Administration
Hampton, VA 23665
September 17, 1979

REFERENCES

1. Seebass, R.; and George, A. R.: Sonic-Boom Minimization. *J. Acoust. Soc. America*, vol. 51, no. 2, pt. 3, Feb. 1972, pp. 686-694.
2. Carlson, Harry W.; Barger, Raymond L.; and Mack, Robert J.: Application of Sonic-Boom Minimization Concepts in Supersonic Transport Design. NASA TN D-7218, 1973.
3. Whitham, G. B.: The Flow Pattern of a Supersonic Projectile. *Commun. Pure & Appl. Math.*, vol. V, no. 3, Aug. 1952, pp. 301-348.
4. Walkden, F.: The Shock Pattern of a Wing-Body Combination, Far From the Flight Path. *Aeronaut. Q.*, vol. IX, pt. 2, May 1958, pp. 164-194.
5. Carlson, Harry W.: Correlation of Sonic-Boom Theory With Wind-Tunnel and Flight Measurements. NASA TR R-213, 1964.
6. Jones, L. B.: Lower Bounds For Sonic Bangs. *J. Roy. Aeronaut. Soc.*, vol. 65, no. 606, June 1961, pp. 433-436.
7. McLean, F. Edward: Some Nonasymptotic Effects On the Sonic Boom of Large Airplanes. NASA TN D-2877, 1965.
8. Carlson, Harry W.; McLean, F. Edward; and Shrout, Barrett L.: A Wind-Tunnel Study of Sonic-Boom Characteristics for Basic and Modified Models of a Supersonic Transport Configuration. NASA TM X-1236, 1966.
9. Hayes, Wallace D.; Haefeli, Rudolph C.; and Kulsrud, H. E.: Sonic Boom Propagation in a Stratified Atmosphere, With Computer Program. NASA CR-1299, 1969.
10. Darden, Christine M.: Minimization of Sonic-Boom Parameters in Real and Isothermal Atmospheres. NASA TN D-7842, 1975.
11. Darden, Christine M.: Sonic-Boom Minimization With Nose-Bluntness Relaxation. NASA TP-1348, 1979.
12. Monaghan, R. J.: An Approximate Solution of the Compressible Laminar Boundary Layer on a Flat Plate. R. & M. No. 2760, British A.R.C., 1953.
13. Harris, Roy V., Jr.: A Numerical Technique for Analysis of Wave Drag at Lifting Conditions. NASA TN D-3586, 1966.
14. Carlson, Harry W.; and Miller, David S.: Numerical Methods for the Design and Analysis of Wings at Supersonic Speeds. NASA TN D-7713, 1974.
15. Shrout, Barrett L.; Mack, Robert J.; and Dollyhigh, Samuel M.: A Wind-Tunnel Investigation of Sonic-Boom Pressure Distributions on Bodies of Revolution at Mach 2.96, 3.83, and 4.63. NASA TN D-6195, 1971.

16. Miller, David S.; Morris, Odell A.; and Carlson, Harry W.: Wind-Tunnel Investigation of Sonic-Boom Characteristics of Two Simple Wing Models at Mach Numbers From 2.3 to 4.63. NASA TN D-6201, 1971.
17. Thomas, Charles L.: Extrapolation of Sonic Boom Pressure Signatures by the Waveform Parameter Method. NASA TN D-6832, 1972.

TABLE I.- NUMERICAL DESCRIPTION OF AIRCRAFT USED FOR DESIGNING

TEST MODELS WAVE-DRAG PROGRAM FORMAT (REF. 12)

[Dimensions in m and m²]

(a) Reference delta

1	-1	-1	-1	5	11	2	19	30	19	30		
773.32												REFA
0.	10.	20.	30.	40.	50.	60.	70.	80.	90.			XAF10
100.												XAF11
28.194	1.981	0.000	34.168									WAFORG1
37.490	4.572	0.000	24.689									WAFORG2
43.891	9.754	0.000	17.678									WAFORG3
50.444	15.240	0.000	11.125									WAFORG4
58.217	21.641	0.000	3.353									WAFORG5
0.	.53	.94	1.24	1.43	1.5	1.43	1.24	.94	.53			WAFORD10
0.												WAFORD11
0.	.53	.94	1.24	1.43	1.5	1.43	1.24	.94	.53			WAFORD20
0.												WAFORD21
0.	.53	.94	1.24	1.43	1.5	1.43	1.24	.94	.53			WAFORD30
0.												WAFORD31
0.	.53	.94	1.24	1.43	1.5	1.43	1.24	.94	.53			WAFORD40
0.												WAFORD41
0.	.53	.94	1.24	1.43	1.5	1.43	1.24	.94	.53			WAFORD50
0.												WAFORD51
0.000	1.524	3.048	4.572	6.096	7.620	9.144	10.668	12.192	13.716			XFUS10
15.240	16.764	18.288	19.812	21.336	22.860	24.384	25.908	27.432	28.956			XFUS11
30.480	32.004	33.528	35.052	36.576	38.100	39.624	41.148	42.672	44.196			XFUS12
0.000	.465	1.068	1.858	2.769	3.716	4.664	5.621	6.578	7.525			FUSA10
8.408	9.244	9.941	10.554	11.037	11.427	11.752	11.910	11.984	11.984			FUSA11
11.966	11.929	11.892	11.845	11.752	11.724	11.706	11.687	11.687	11.687			FUSA12
44.196	45.720	47.244	48.768	50.292	51.816	53.340	54.864	56.388	57.912			XFUS20
59.436	60.960	62.484	64.008	65.532	67.056	68.580	70.104	71.628	73.152			XFUS21
74.676	76.200	77.724	79.248	80.772	82.296	83.820	85.344	86.868	88.392			XFUS22
11.687	11.641	11.594	11.520	11.390	11.241	11.037	10.777	10.498	10.191			FUSA20
9.811	9.458	9.095	8.659	8.659	8.659	8.659	8.659	8.659	8.659			FUSA21
8.659	8.659	8.659	8.659	8.659	8.659	8.659	8.659	8.659	8.659			FUSA22

TABLE I.- Continued

(b) Reference arrow

1	-1	-1		-1	5	12	2	19	30	19	18		
982.45													REFA
0.	5.	10.	20.	30.	40.	50.	60.	70.	80.				XAF10
90.	100.												XAF12
24.994	1.829	0.000	48.768										WAFORG1
35.052	4.877	0.000	38.710										WAFORG2
52.121	9.754	0.000	23.043										WAFORG3
69.037	14.630	0.000	9.754										WAFORG4
78.334	20.117	0.000	4.328										WAFORG5
0.	.575	.78	1.03	1.17	1.26	1.3	1.24	1.08	.82				WAFORD10
.45	0.												WAFORD12
0.	.575	.78	1.03	1.17	1.26	1.3	1.24	1.08	.82				WAFORD20
.45	0.												WAFORD22
0.	.575	.78	1.03	1.17	1.26	1.3	1.24	1.08	.82				WAFORD30
.45	0.												WAFORD32
0.	.575	.78	1.03	1.17	1.26	1.3	1.24	1.08	.82				WAFORD40
.45	0.												WAFORD42
0.	.575	.78	1.03	1.17	1.26	1.3	1.24	1.08	.82				WAFORD50
.45	0.												WAFORD52
0.000	3.048	6.096	9.144	12.192	15.240	18.288	21.336	24.384	27.432				XFUS10
30.480	33.528	36.576	39.624	42.672	45.720	48.768	51.816	54.864	57.912				XFUS20
60.960	64.008	67.056	70.104	73.152	76.200	79.248	82.296	85.344	88.392				XFUS30
0.000	1.115	2.880	4.738	6.503	8.268	9.848	11.241	11.613	11.474				FUSA10
10.870	10.312	9.848	9.755	9.848	9.894	9.941	9.941	9.848	9.708				FUSA20
9.476	9.012	8.547	7.711	6.689	5.481	5.481	5.481	5.481	5.481				FUSA30
88.392	91.440	94.488	97.536	100.584	103.632	106.680	109.728	112.776	115.824				XFUS40
118.872	121.920	124.968	128.016	131.064	134.112	137.160	140.208						XFUS50
5.481	5.481	5.481	5.481	5.481	5.481	5.481	5.481	5.481	5.481				FUSA40
5.481	5.481	5.481	5.481	5.481	5.481	5.481	5.481	5.481	5.481				FUSA50

TABLE I.- Continued

(c) Mach 2.7 low-boom arrow

1	-1	-1		-1	5	11	3	19	20	19	20	19	25	
1482.73														REFA
0.	10.	20.	30.	40.	50.	60.	70.	80.	90.					XAF 10
100.														XAF 11
17.526	2.286	.295	65.627											WAFORG 1
54.864	9.754	1.262	31.090											WAFORG 2
64.008	12.192	1.578	22.860											WAFORG 3
71.018	14.630	1.893	16.764											WAFORG 4
86.868	24.384	3.156	4.572											WAFORG 5
0.	.378	.672	.882	1.008	1.050	1.008	.882	.672	.378					WAFORD10
0.														WAFORD11
0.	.353	.635	.852	.975	1.023	1.005	.873	.675	.394					WAFORD20
0.														WAFORD21
0.	.400	.698	.908	1.044	1.093	1.080	.958	.737	.453					WAFORD30
0.														WAFORD31
0.	.464	.782	1.032	1.186	1.266	1.225	1.075	.820	.545					WAFORD40
0.														WAFORD41
0.	.658	1.100	1.400	1.625	1.716	1.725	1.583	1.350	.992					WAFORD50
0.														WAFORD51
0.000	1.524	3.048	4.572	6.096	7.620	9.144	10.668	12.192	13.716					XFUS 10
15.240	16.764	18.288	19.812	21.336	22.860	24.384	25.908	27.432	28.956					XFUS 11
0.000	.074	.307	.901	2.573	4.069	5.583	7.116	8.556	9.857					FUSA 10
11.055	12.161	13.202	14.121	14.920	15.728	16.332	16.815	17.168	17.419					FUSA 11
28.956	30.480	32.004	33.528	35.052	36.576	38.100	39.624	41.148	42.672					XFUS 20
44.196	45.720	47.244	48.768	50.292	51.816	53.340	54.864	56.388	57.912					XFUS 21
17.419	17.549	17.577	17.512	17.391	17.326	17.196	16.927	16.750	16.527					FUSA 20
16.332	16.091	15.831	15.598	15.366	15.152	14.967	14.632	14.298	13.917					FUSA 21
57.912	59.436	60.960	62.484	64.008	65.532	67.056	68.580	70.104	71.628					XFUS 30
73.152	74.676	76.200	77.724	79.248	80.772	82.296	83.820	85.344	86.868					XFUS 31
88.392	89.916	91.440	92.964	94.488										XFUS 32
13.917	13.499	13.118	12.542	11.957	11.492	10.898	10.349	9.838	9.383					FUSA 30
8.928	8.463	7.980	7.534	7.079	6.652	6.206	5.797	5.444	5.091					FUSA 31
4.785	4.589	4.227	4.116	4.041										FUSA 32

TABLE I.- Continued

(d) Mach 2.7 low-boom blunt-apex arrow^a

1	-1	-1		-1	9	11	3	19	20	19	20	19	27		
1541.91															REFA
0.	10.	20.	30.	40.	50.	60.	70.	80.	90.						XAF 10
100.0															XAF 11
4.478	1.829	.297	82.086												WAFORG1
6.096	2.134	.346	80.467												WAFORG2
13.716	3.200	.519	72.847												WAFORG3
22.860	4.267	.693	63.703												WAFORG4
51.511	8.534	1.385	36.271												WAFORG5
60.960	10.668	1.731	27.432												WAFORG6
68.275	12.802	2.078	20.726												WAFORG7
74.066	14.935	2.424	15.545												WAFORG8
86.868	21.336	3.463	4.572												WAFORG9
0.0	.36	.64	.84	.96	1.0	.96	.84	.64	.36						WAFORD10
0.0															WAFORD11
0.	.365	.634	.842	.958	.991	.956	.842	.644	.362						WAFORD20
0.0															WAFORD21
0.	.364	.634	.839	.957	.993	.957	.842	.643	.359						WAFORD30
0.0															WAFORD31
0.	.366	.654	.852	.966	1.001	.966	.844	.643	.367						WAFORD40
0.0															WAFORD41
0.	.381	.675	.895	1.014	1.046	1.012	.888	.673	.383						WAFORD50
0.0															WAFORD51
0.	.389	.703	.920	1.058	1.104	1.070	.927	.699	.526						WAFORD60
0.0															WAFORD61
0.	.434	.752	.987	1.155	1.203	1.149	1.000	.758	.439						WAFORD70
0.0															WAFORD71
0.	.459	.833	1.111	1.245	1.297	1.248	1.089	.851	.532						WAFORD80
0.															WAFORD81
0.	1.292	1.792	2.067	2.242	2.259	2.158	2.033	1.667	1.100						WAFORD90
0.0															WAFORD91
0.000	1.524	3.048	4.572	6.096	7.620	9.144	10.668	12.192	13.716						XFUS 10
15.240	16.764	18.288	19.812	21.336	22.860	24.384	25.908	27.432	28.956						XFUS 11
0.000	.160	.463	.846	1.682	2.863	4.078	5.316	6.349	7.206						FUSA 10
7.884	8.547	9.154	9.684	10.135	10.559	10.878	11.057	11.255	11.401						FUSA 11
28.956	30.480	32.004	33.528	35.052	36.576	38.100	39.624	41.148	42.672						XFUS 20
44.196	45.720	47.244	48.768	50.292	51.816	53.340	54.864	56.388	57.912						XFUS 21
11.401	11.584	11.584	11.603	11.603	11.603	11.621	11.621	11.621	11.621						FUSA 20
11.621	11.621	11.621	11.603	11.603	11.603	11.603	11.603	11.584	11.639						FUSA 21
57.912	59.436	60.960	62.484	64.008	65.532	67.056	68.580	70.104	71.628						XFUS 30
73.152	74.676	76.200	77.724	79.248	80.772	82.296	83.820	85.344	86.868						XFUS 31
88.392	89.916	91.440	92.964	94.488	96.012	97.536									XFUS 32
11.639	11.584	11.565	11.419	11.274	11.003	10.860	10.542	10.194	9.903						FUSA 30
9.400	8.829	8.245	7.726	7.137	6.613	6.176	5.793	5.422	5.124						FUSA 31
4.799	4.600	4.439	4.281	4.159	4.126	4.104									FUSA 32.

$$a_0 \leq y \leq 3.2004; \quad x_{7e} = 13.716(y/3.2004)^2.$$

TABLE I.- Concluded

(e) Mach 1.5 low-boom arrow

1 -1 -1 0 0 0 -1 11 11 3 19 21 19 21 19 24											REFA
1405.34	0.	10.	20.	30.	40.	50.	60.	70.	80.	90.	
0.											XAF 10
100.											XAF 11
19.159	1.676	.380	71.062								WAFORG1
24.384	2.134	.484	65.532								WAFORG2
33.528	4.267	.967	56.388								WAFORG3
43.282	6.401	1.451	46.634								WAFORG4
53.340	8.534	1.935	36.576								WAFORG5
63.398	10.668	2.419	26.771								WAFORG6
71.933	12.802	2.903	18.492								WAFORG7
77.114	14.935	3.386	13.564								WAFORG8
80.467	17.069	3.870	10.464								WAFORG9
83.515	19.202	4.354	7.672								WAFORG10
86.868	21.336	4.838	4.572								WAFORG11
0.0	.36	.64	.84	.96	1.0	.96	.64	.64	.36		WAFORD 1
0.0											WAFORD 1
0.0	.371	.644	.860	.983	1.030	.995	.873	.666	.384		WAFORD 2
0.0											WAFORD 2
0.0	.403	.705	.934	1.072	1.120	1.081	.951	.722	.414		WAFORD 3
0.0											WAFORD 3
0.0	.432	.761	1.012	1.167	1.221	1.185	1.037	.783	.449		WAFORD4
0.0											WAFORD 4
0.0	.472	.818	1.082	1.256	1.321	1.283	1.128	.849	.448		WAFORD 5
0.0											WAFORD 5
0.0	.528	.889	1.174	1.365	1.440	1.395	1.213	.902	.537		WAFORD 6
0.0											WAFORD 6
0.0	.593	1.012	1.333	1.523	1.585	1.523	1.308	.985	.598		WAFORD 7
0.0											WAFORD 7
0.0	.674	1.098	1.410	1.607	1.674	1.612	1.385	1.056	.643		WAFORD 8
0.0											WAFORD 8
0.0	.746	1.194	1.504	1.700	1.784	1.722	1.489	1.169	.721		WAFORD 9
0.0											WAFORD 9
0.0	.830	1.272	1.604	1.848	1.942	1.843	1.614	1.267	.800		WAFORD10
0.0											WAFORD10
0.0	.883	1.425	1.842	2.050	2.058	1.958	1.750	1.367	.867		WAFORD11
0.0											WAFORD11
0.000	1.524	3.048	4.572	6.096	7.620	9.144	10.668	12.192	13.716		XFUS10
15.240	16.764	18.288	19.812	21.336	22.860	24.384	25.908	27.432	28.956		XFUS11
30.480											XFUS12
0.000	.092	.353	.776	1.394	2.065	2.886	3.825	4.764	5.599		FUSA 10
6.502	7.370	8.183	8.974	9.616	10.298	10.825	11.201	11.565	11.880		FUSA 11
12.124											FUSA 12
30.480	32.004	33.528	35.052	36.576	38.100	39.624	41.148	42.672	44.196		XFUS20
45.720	47.244	48.768	50.292	51.816	53.340	54.864	56.388	57.912	59.436		XFUS21
60.960											XFUS22
12.124	12.351	12.503	12.656	12.733	12.752	12.771	12.618	12.503	12.369		FUSA 20
12.236	11.918	11.639	11.328	11.057	10.789	10.525	10.454	10.194	9.988		FUSA 21
9.836											FUSA 22
60.960	62.484	64.008	65.532	67.056	68.580	70.104	71.628	73.152	74.676		XFUS30
76.200	77.724	79.248	80.772	82.296	83.820	85.344	86.868	88.392	89.916		XFUS31
91.440	92.964	94.488	96.012								XFUS32
9.836	9.717	9.583	9.466	9.334	9.185	9.185	9.185	9.153	9.185		FUSA 30
9.153	9.136	9.136	9.104	9.136	9.104	8.813	8.167	7.355	6.002		FUSA 31
4.140	4.140	4.140	4.140								FUSA 32

TABLE II.- ANGLE-OF-ATTACK AND PRISM-ANGLE SETTINGS

Model	Mach number											
	1.5		2.6		2.7		2.8					
	α	θ	α	θ	α	θ	α	θ				
Reference delta	3°27'	2°5'	-	-	3°26'	2°51'	-	-				
Reference arrow	4°14'	3°0'	-	-	2°46'	2°14'	-	-				
M=2.7 Low-boom arrow	-	-	● 1°46'	1°12'	1°38'	1°6'	● 1°34'	1°6'				
	-	-	▲ 2°13'	1°30'	2°2'	1°23'	▲ 1°57'	1°22'				
	-	-	● 2°40'	1°48'	2°27'	1°40'	● 2°21'	1°38'				
M=2.7 Low-boom blunt-apex arrow	-	-	-	-	1°48'	1°12'	-	-				
	-	-	-	-	2°15'	1°30'	-	-				
	-	-	-	-	2°42'	1°48'	-	-				
M=1.5 Low-boom arrow	2°42'	1°32'	-	-	-	-	-	-				
	▲ 3°23'	1°56'	-	-	-	-	-	-				
	4°3'	2°19'	-	-	-	-	-	-				

- Test not made

● Test made but data not used in report

▲ Angle which theoretically produces a full-scale

lift of 272 155 kg (600 000 lb)

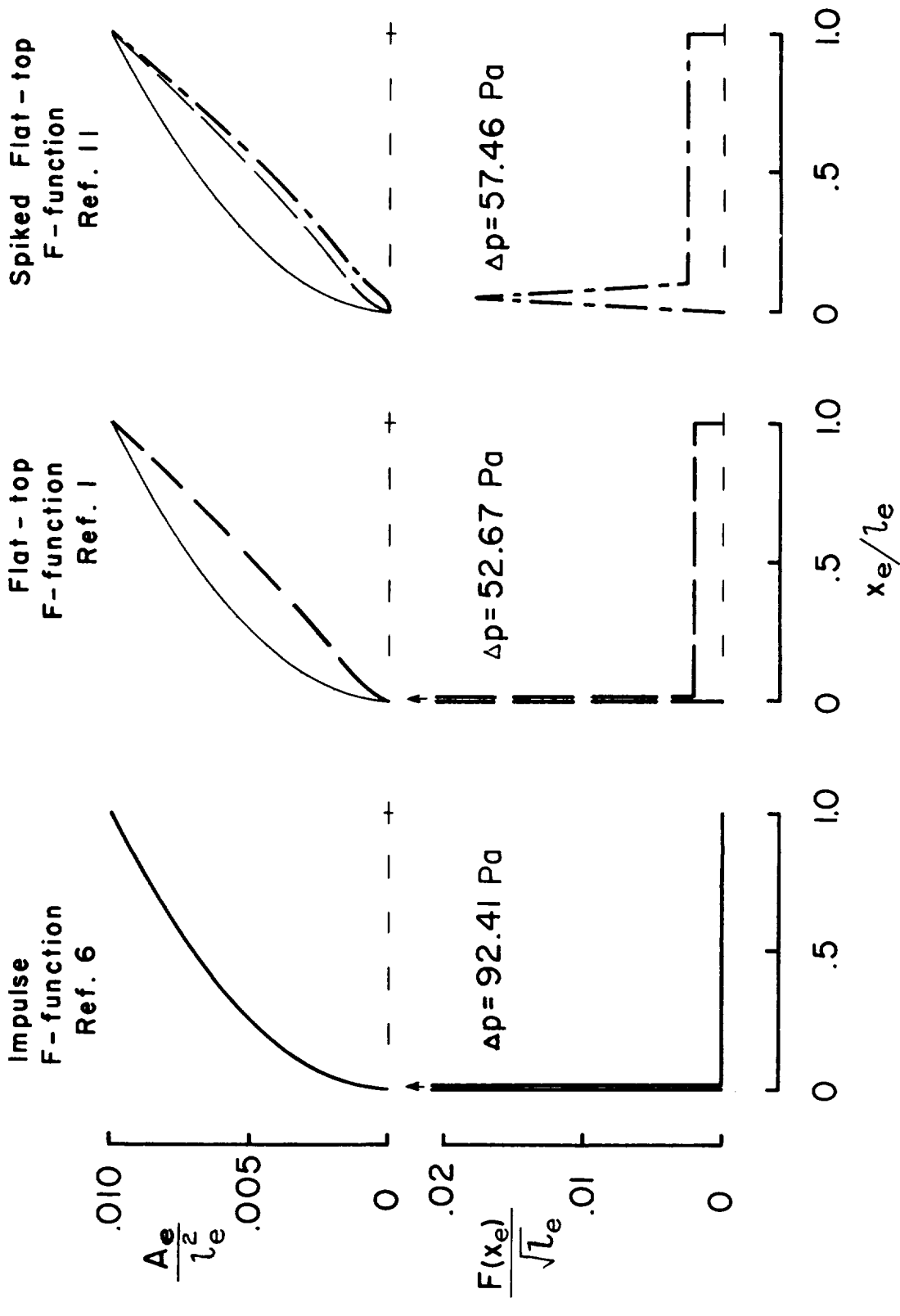


Figure 1.- Effective area and F-functions from minimization methods of references 1, 6, and 11. Δp is calculated for $h = 18\,288 \text{ m}$ (60 000 ft).

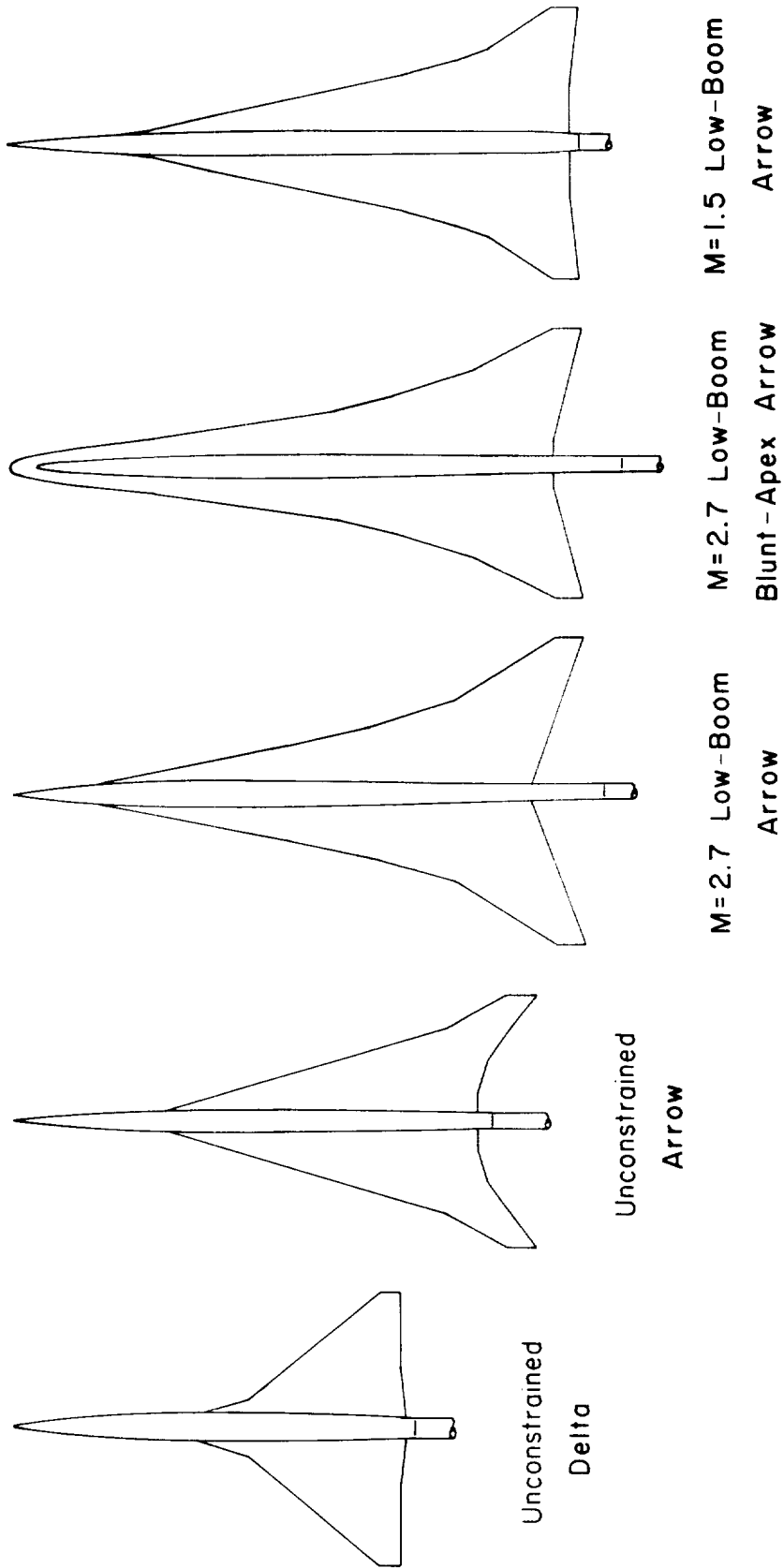
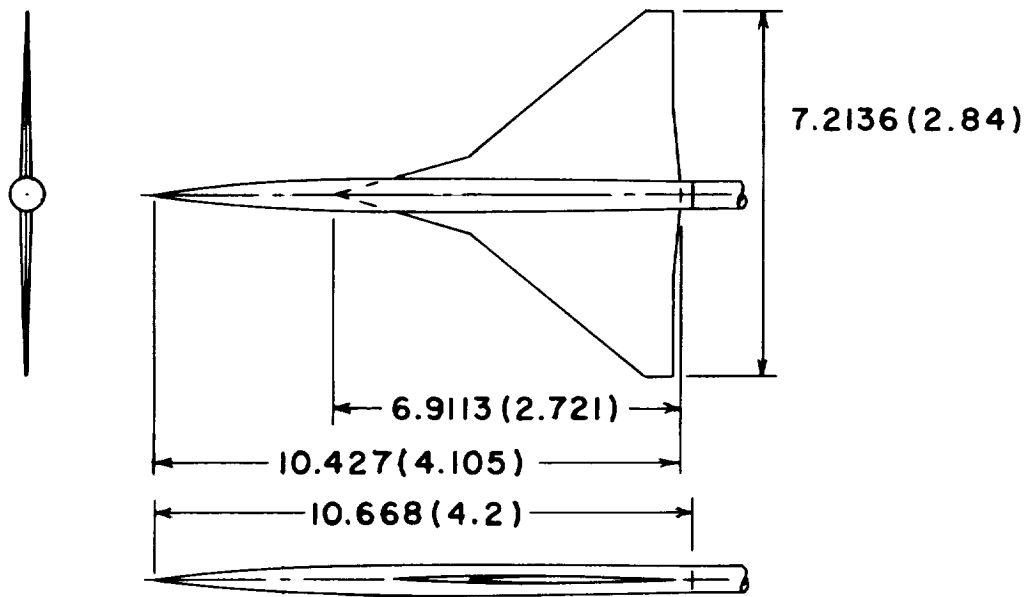
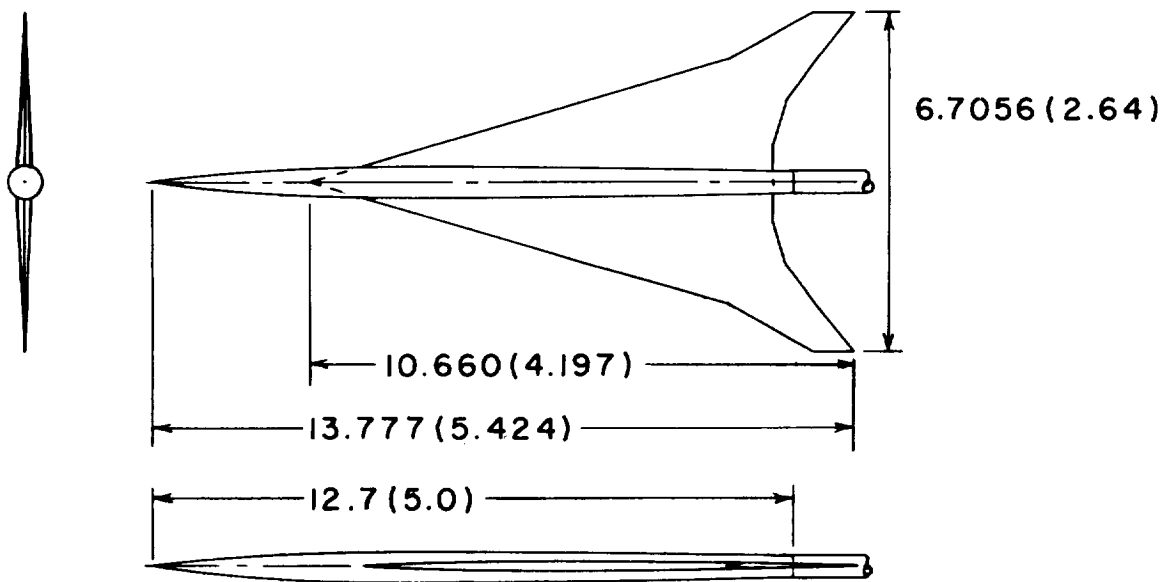


Figure 2.- Models used in sonic-boom minimization study.



(a) Reference delta-wing model.



(b) Reference arrow-wing model.

Figure 3.- Unconstrained wind-tunnel models. Dimensions in cm (in.).

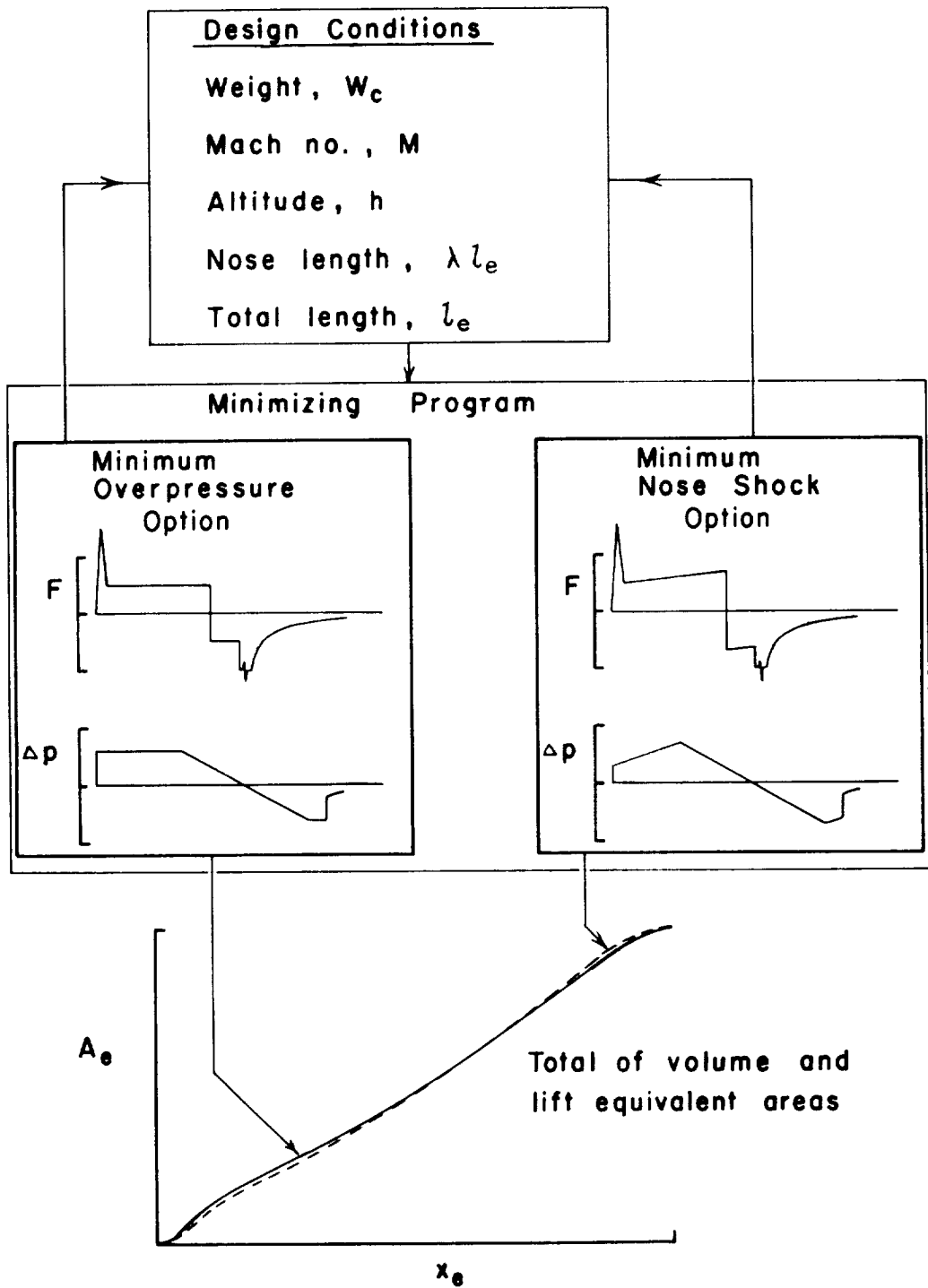


Figure 4.- Schematic outline of minimization process.

Design Conditions

$M = 2.7$
 $W_c = 272\ 155\ \text{kg} (600\ 000\ \text{lb})$
 $h = 18\ 288\ \text{m} (60\ 000\ \text{ft})$
 $l_e = 1 = 91.44\ \text{m} (300\ \text{ft})$
 $\lambda = 0.1 ; K_r = 1.9$
 $\Delta p \leq 50\ \text{Pa} (1.044\ \text{lbf/ft}^2)$

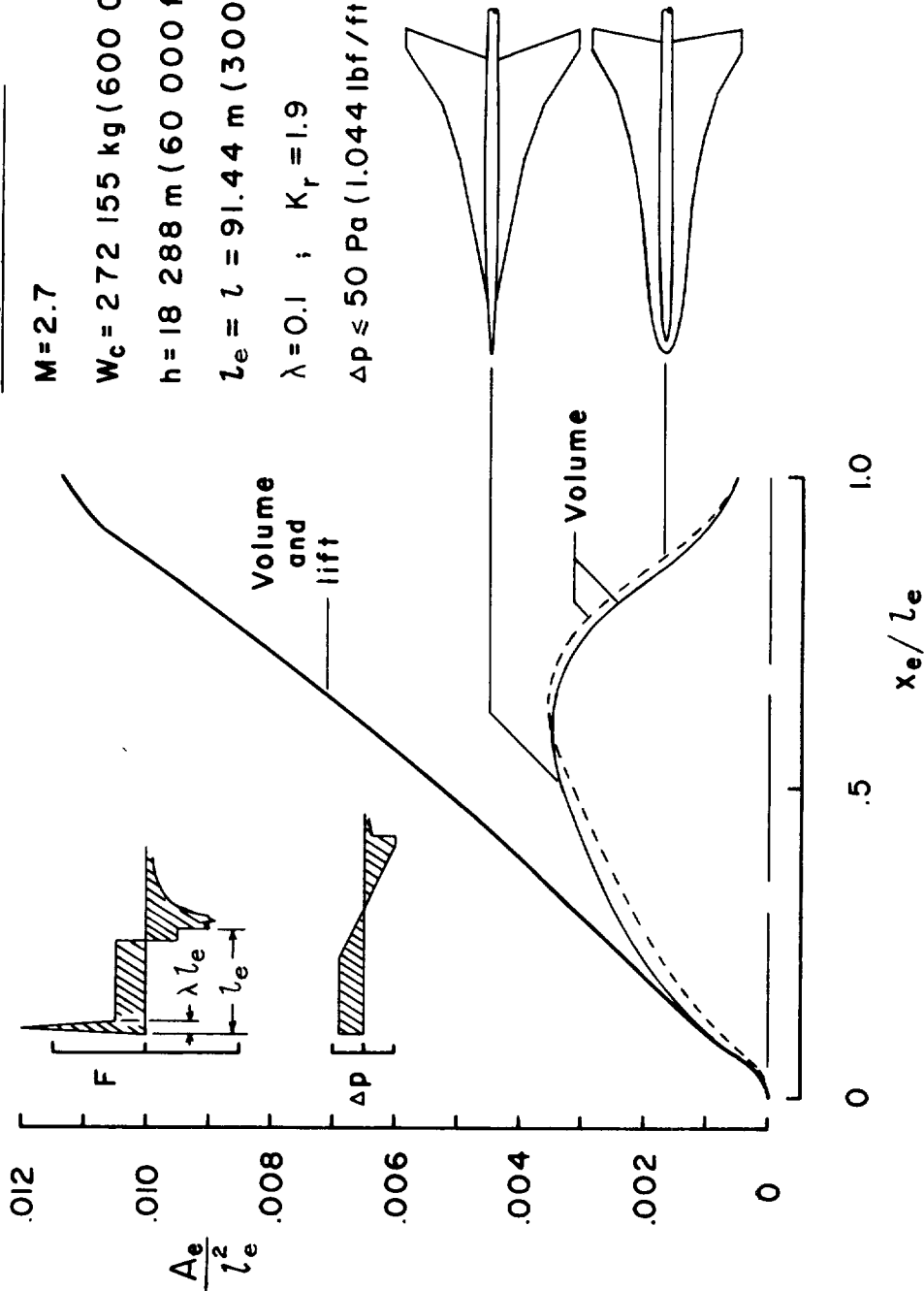


Figure 5.- Example of design procedure for two models which give specified minimum boom at $M = 2.7$.

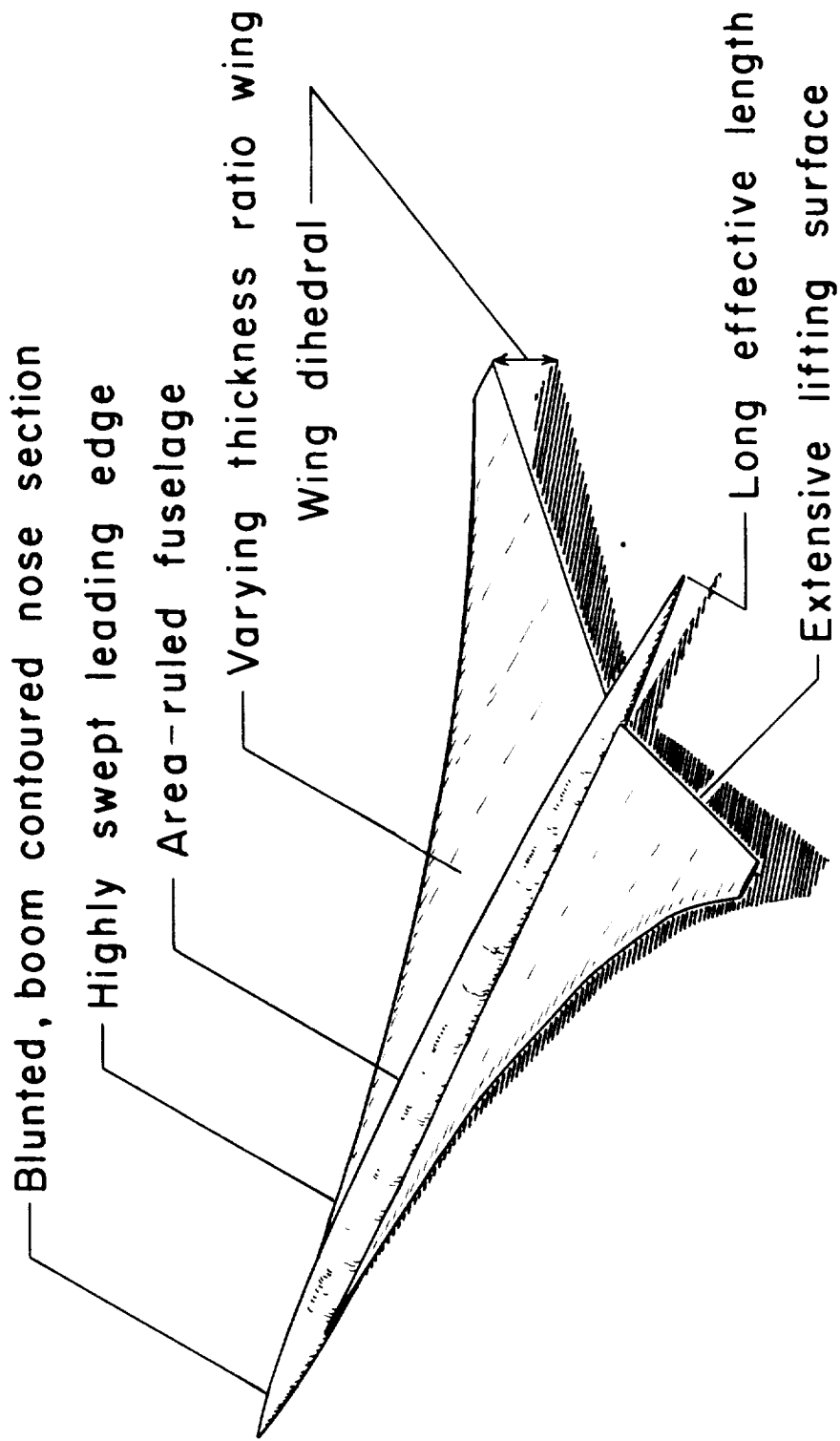
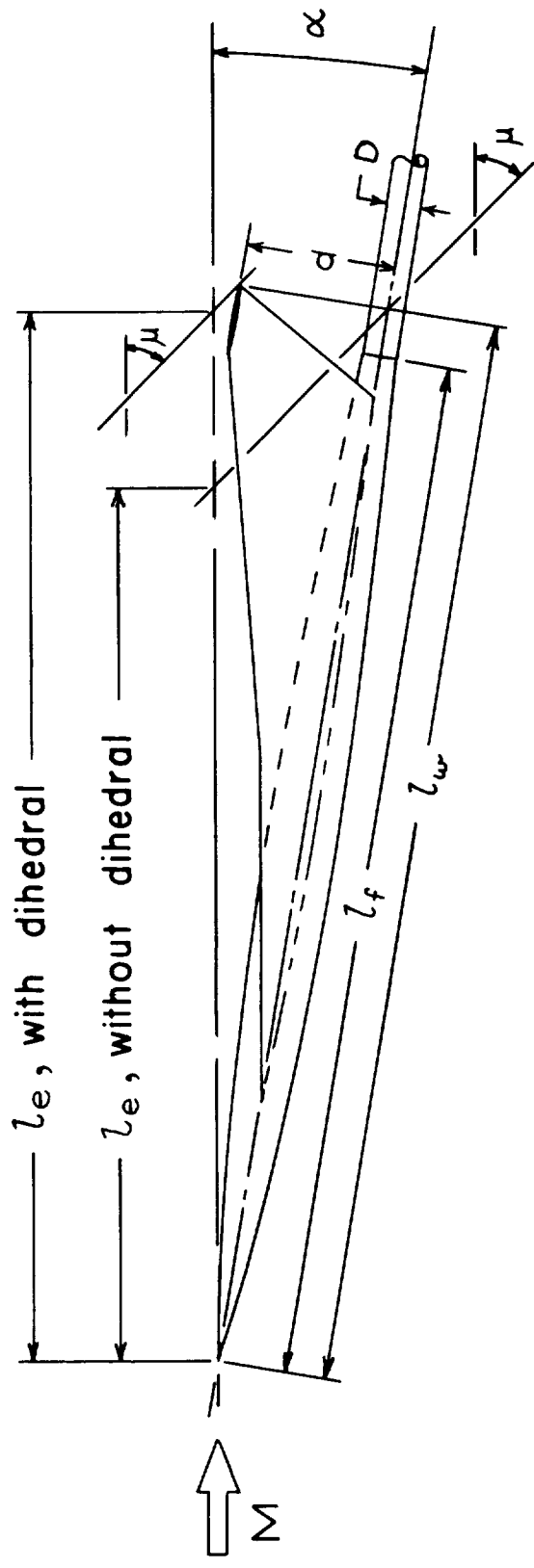
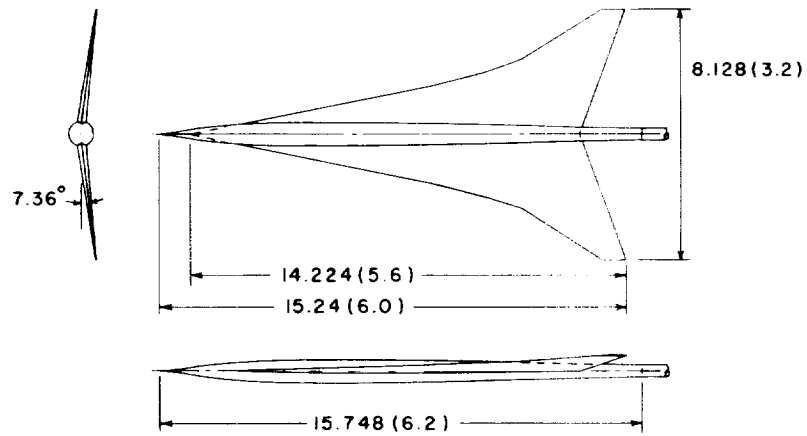


Figure 6.- Features of low-boom study models.

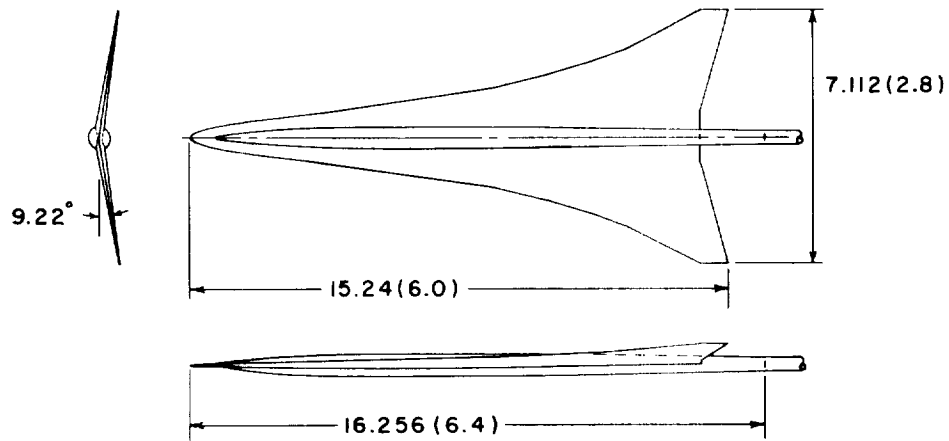


$$l_e = l_w \cos \alpha (1 - \beta \tan \alpha) + d \cos \alpha (\beta + \tan \alpha)$$

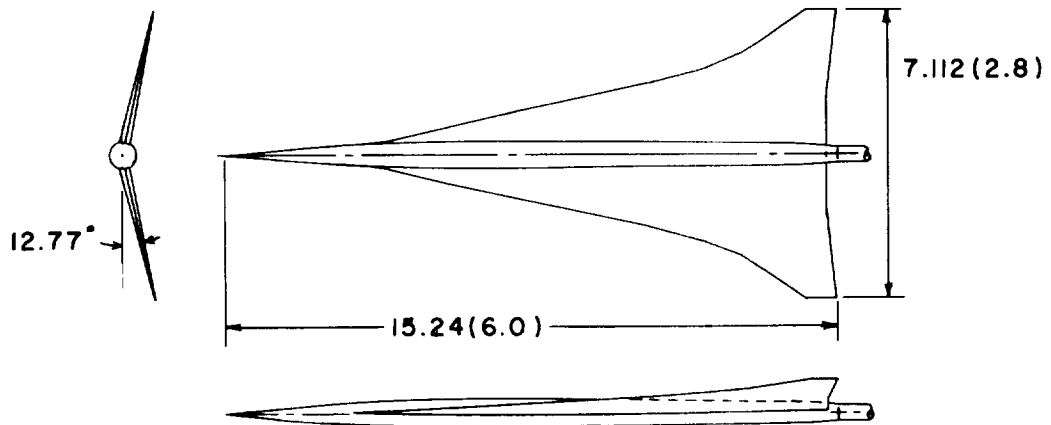
Figure 7.- Side view of model showing effect of dihedral on effective length.



(a) Arrow-wing model designed for minimum boom at $M = 2.7$.

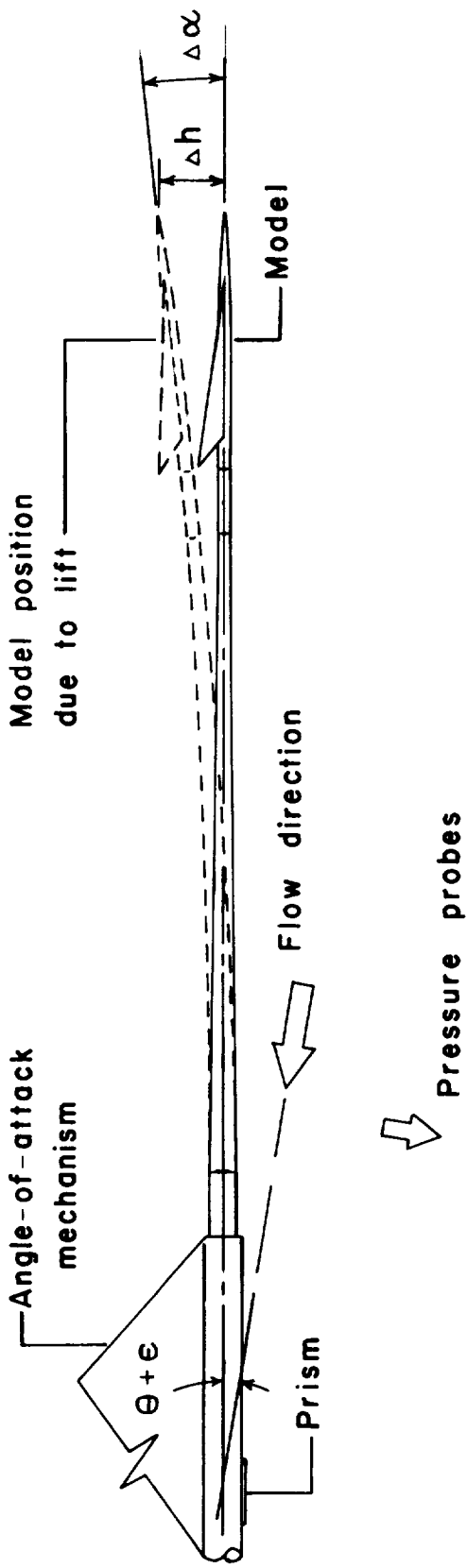


(b) Blunted arrow-wing model designed for minimum boom at $M = 2.7$.



(c) Arrow-wing model designed for minimum boom at $M = 1.5$.

Figure 8.- Low-boom wind-tunnel models. Dimensions in cm (in.).



$$\alpha = \theta + \Delta \alpha$$

$$\Delta \alpha = k C_{L\alpha} \alpha q S$$

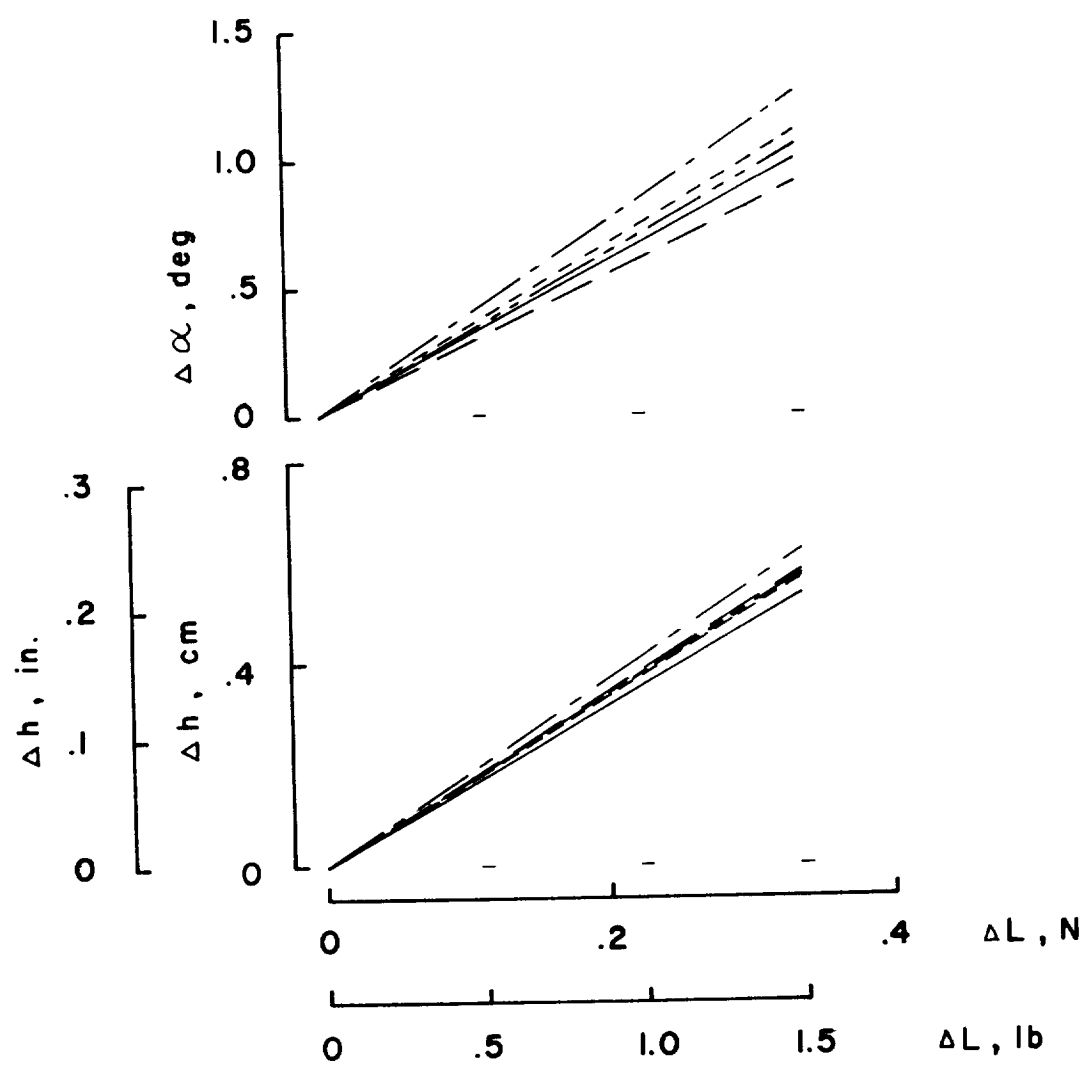
$$k = \Delta \alpha / \Delta L \quad \text{from figure 9(b)}$$

$$\theta = \alpha (1.0 - k C_{L\alpha} q S)$$

(a) Schematic of model, sting, and sting support.

Figure 9.- Corrections due to sting flexure.

Model		
Reference delta		—————
Reference arrow		- - - - -
M=2.7 Low-boom arrow		- - - - -
M=2.7 Low-boom blunted arrow		- - - - -
M=1.5 Low-boom arrow		- - - - -



(b) Deflection curves.

Figure 9.- Concluded.

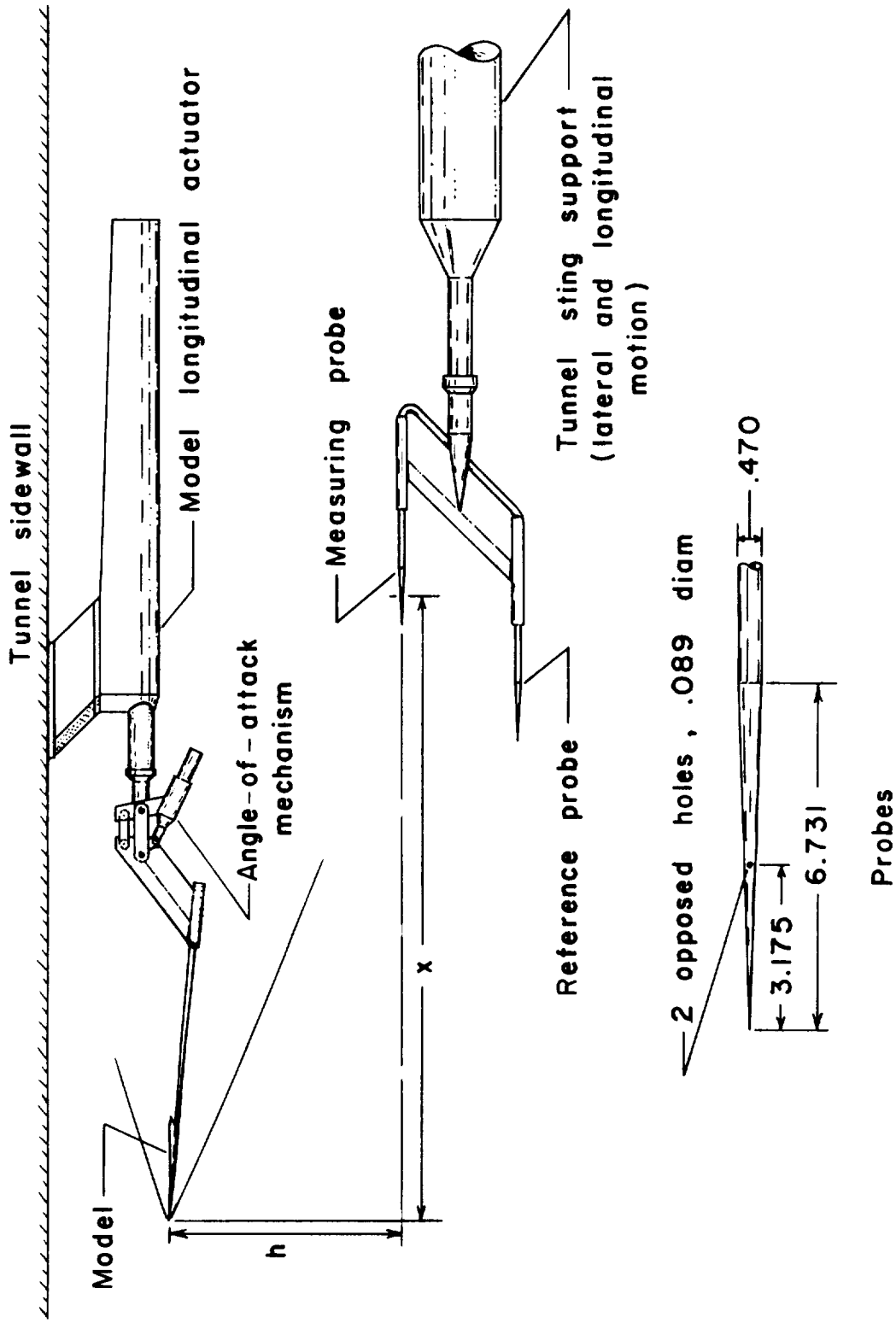
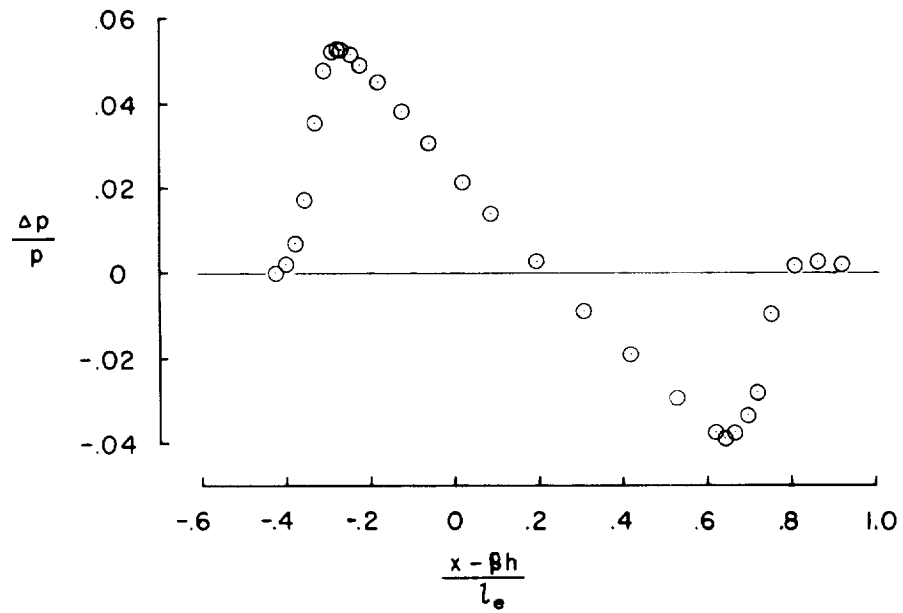
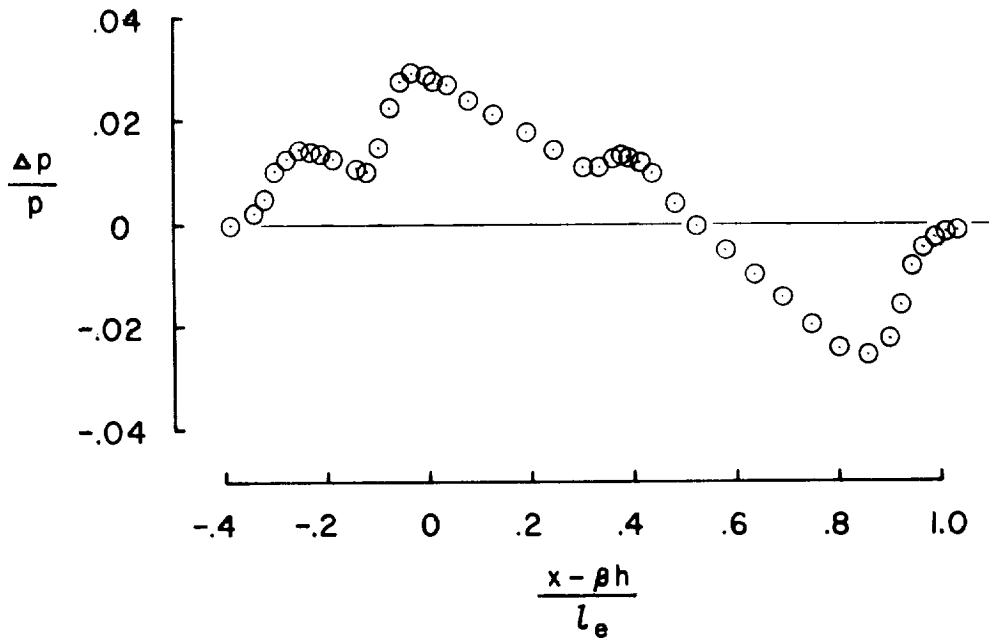


Figure 10.- Schematic of test apparatus. All dimensions are in centimeters.

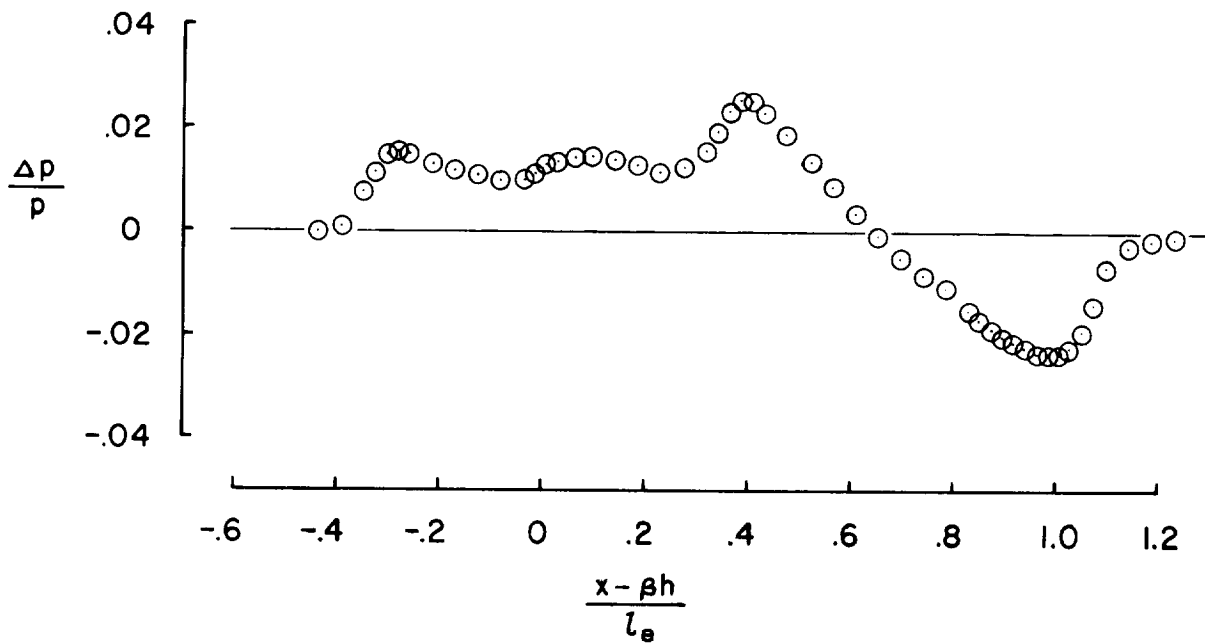


(a) Reference delta-wing model.

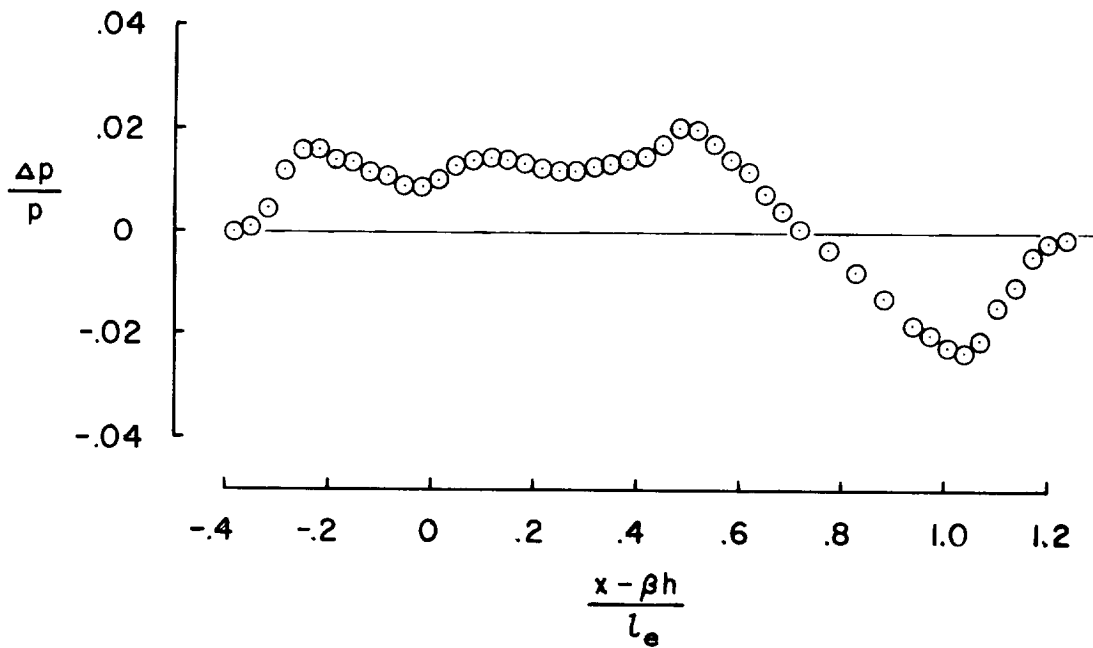


(b) Reference arrow-wing model.

Figure 11.- Measured pressure signatures at $M = 2.7$, $\alpha = \alpha_D$, and $h/l_e = 3$.

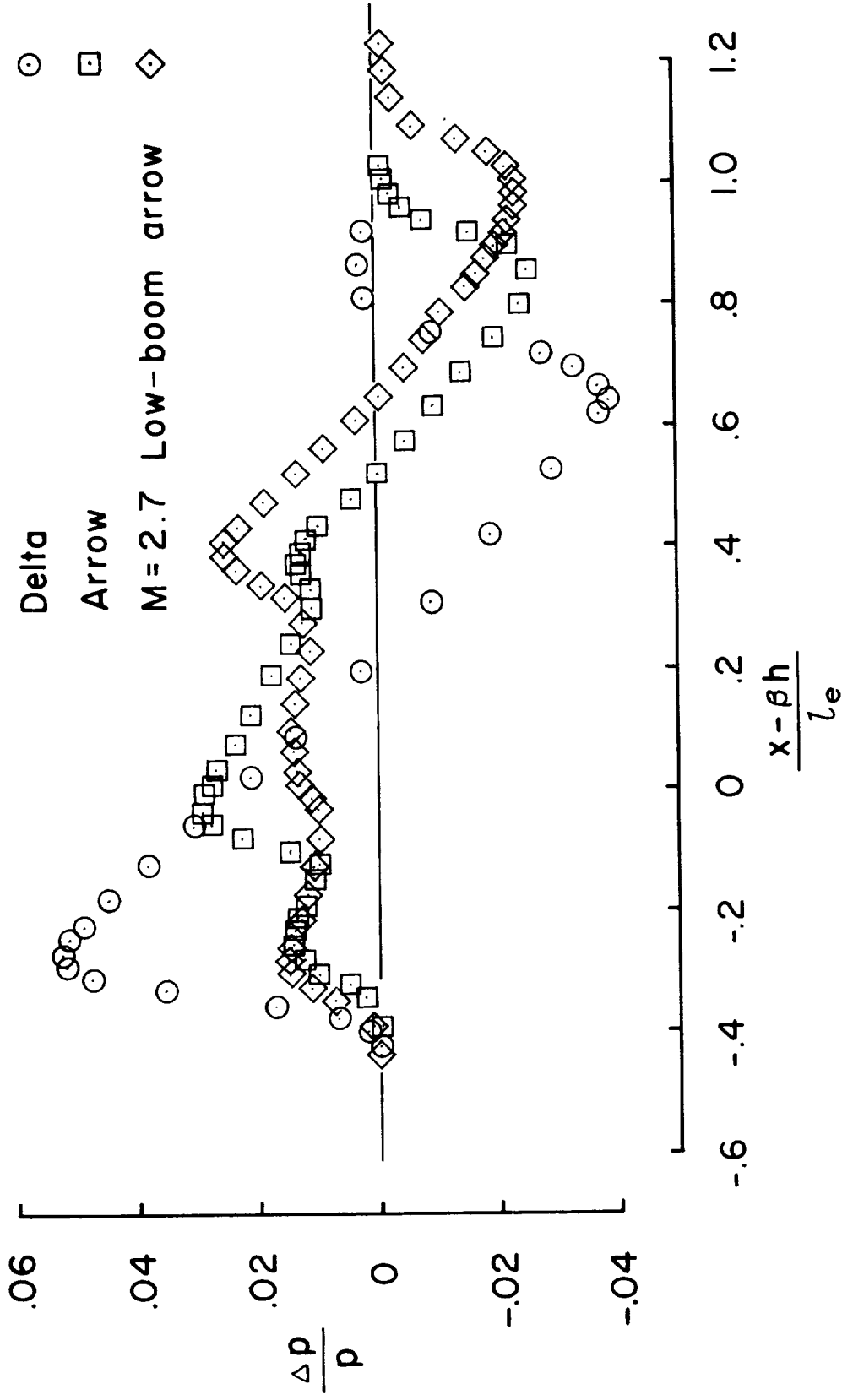


(c) Mach 2.7 low-boom arrow-wing model.



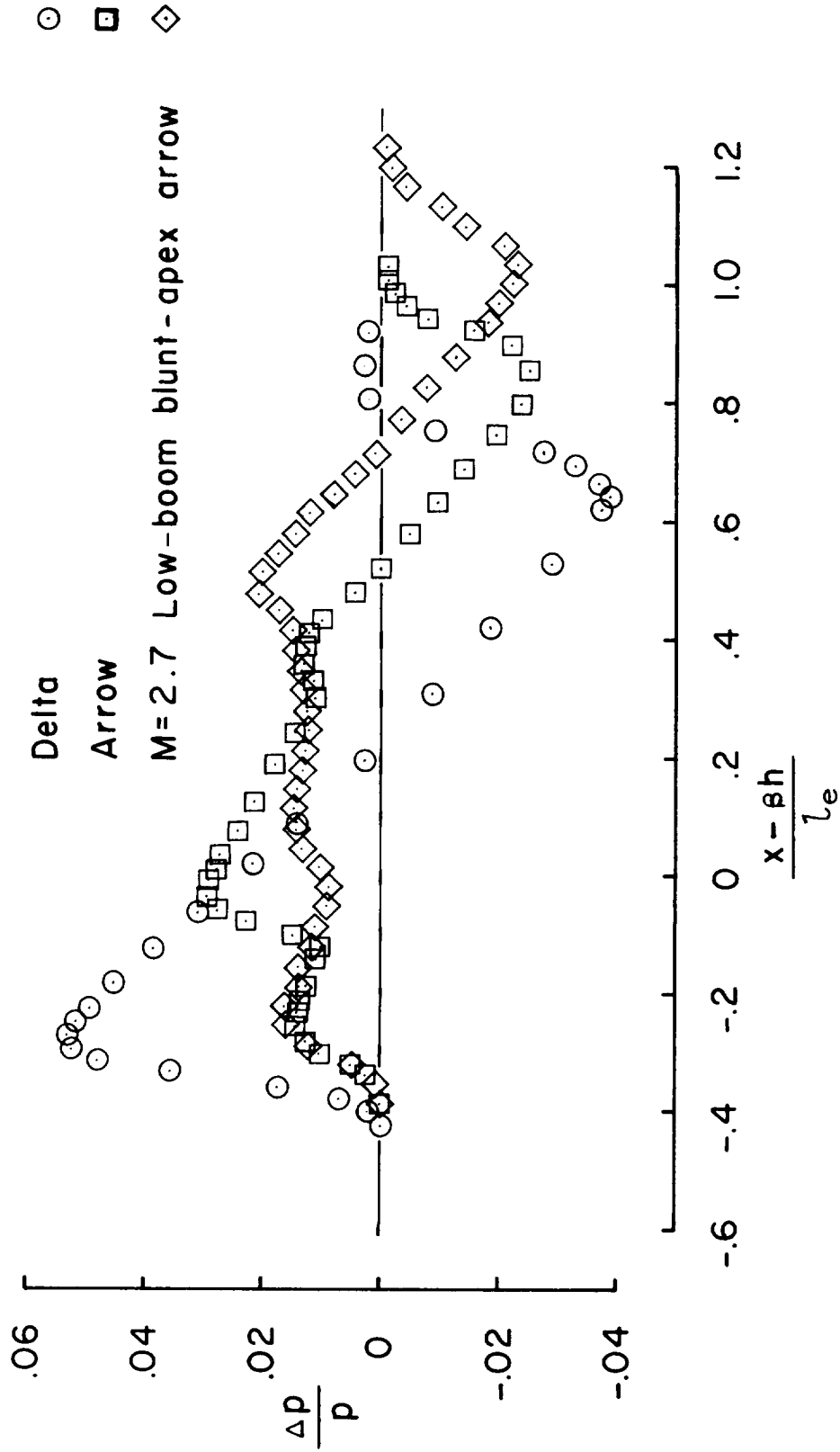
(d) Mach 2.7 low-boom blunt-apex arrow-wing model.

Figure 11.- Continued.



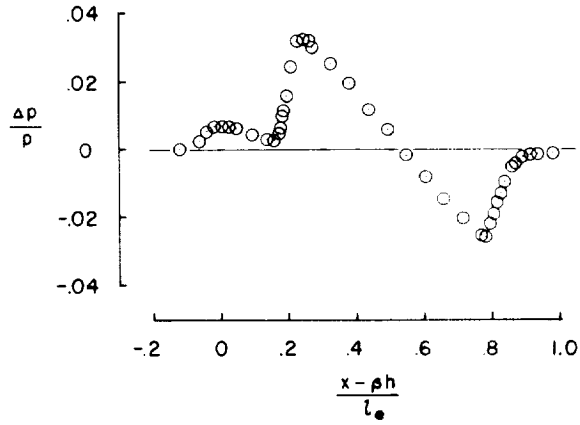
(e) Reference models and Mach 2.7 low-boom arrow-wing model.

Figure 11.- Continued.

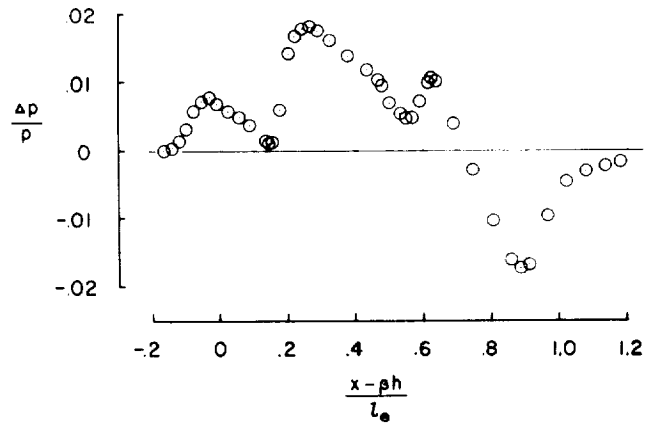


(f) Reference models and Mach 2.7 low-boom blunt-apex arrow-wing model.

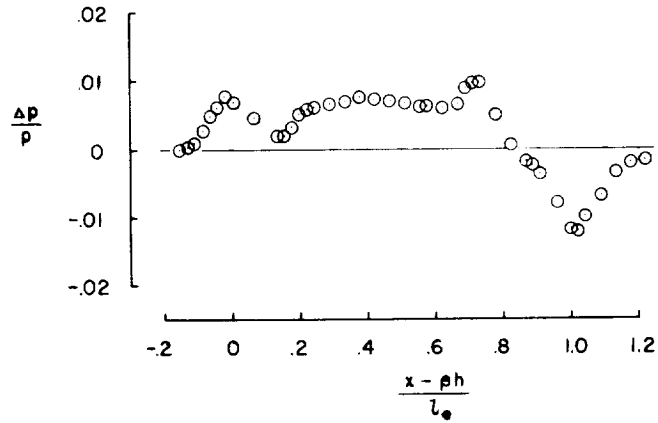
Figure 11.- Concluded.



(a) Reference delta-wing model.

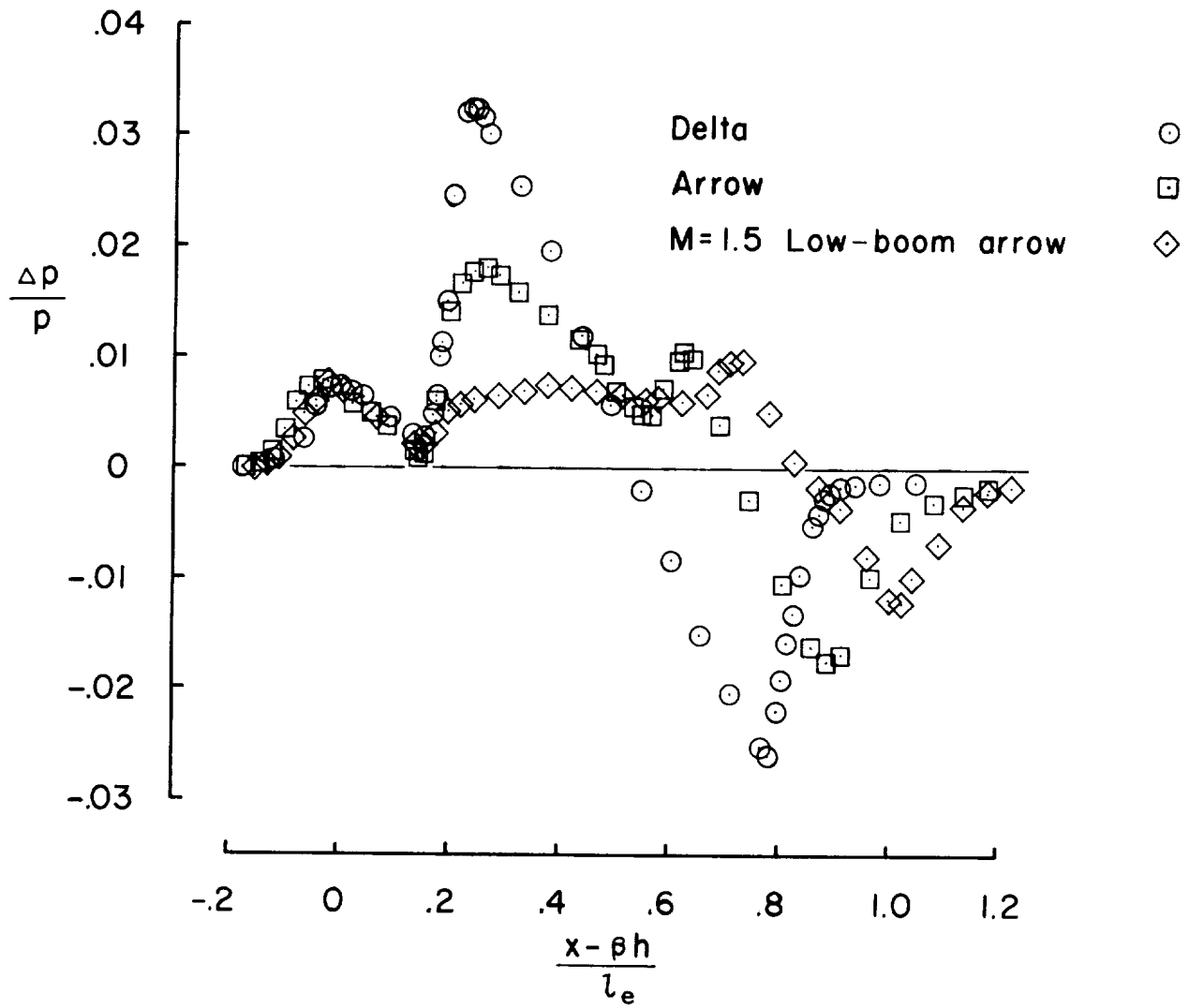


(b) Reference arrow-wing model.



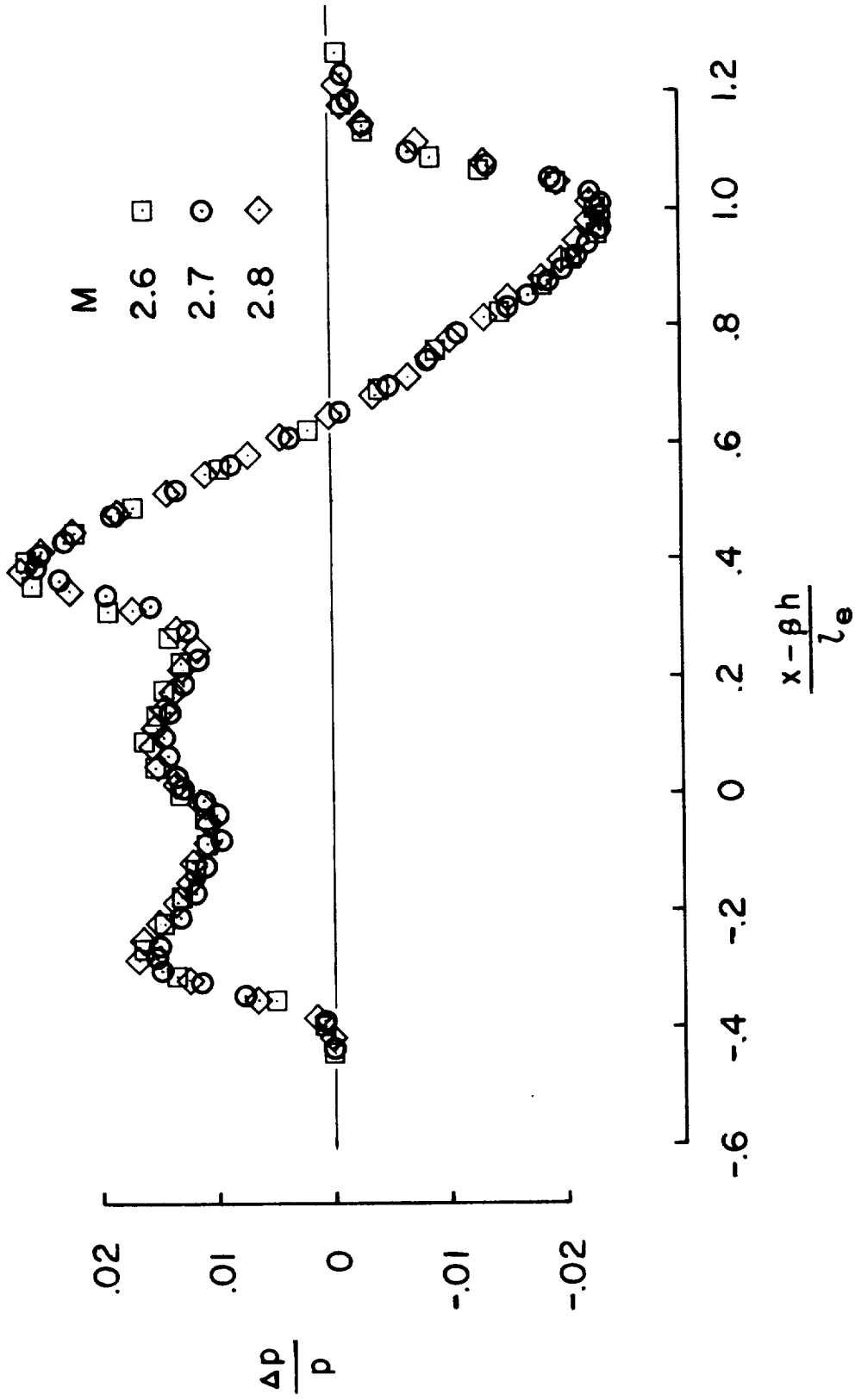
(c) Mach 1.5 low-boom arrow-wing model.

Figure 12.- Measured pressure signatures at $M = 1.5$, $\alpha = \alpha_D$, and $h/l_e = 3$.



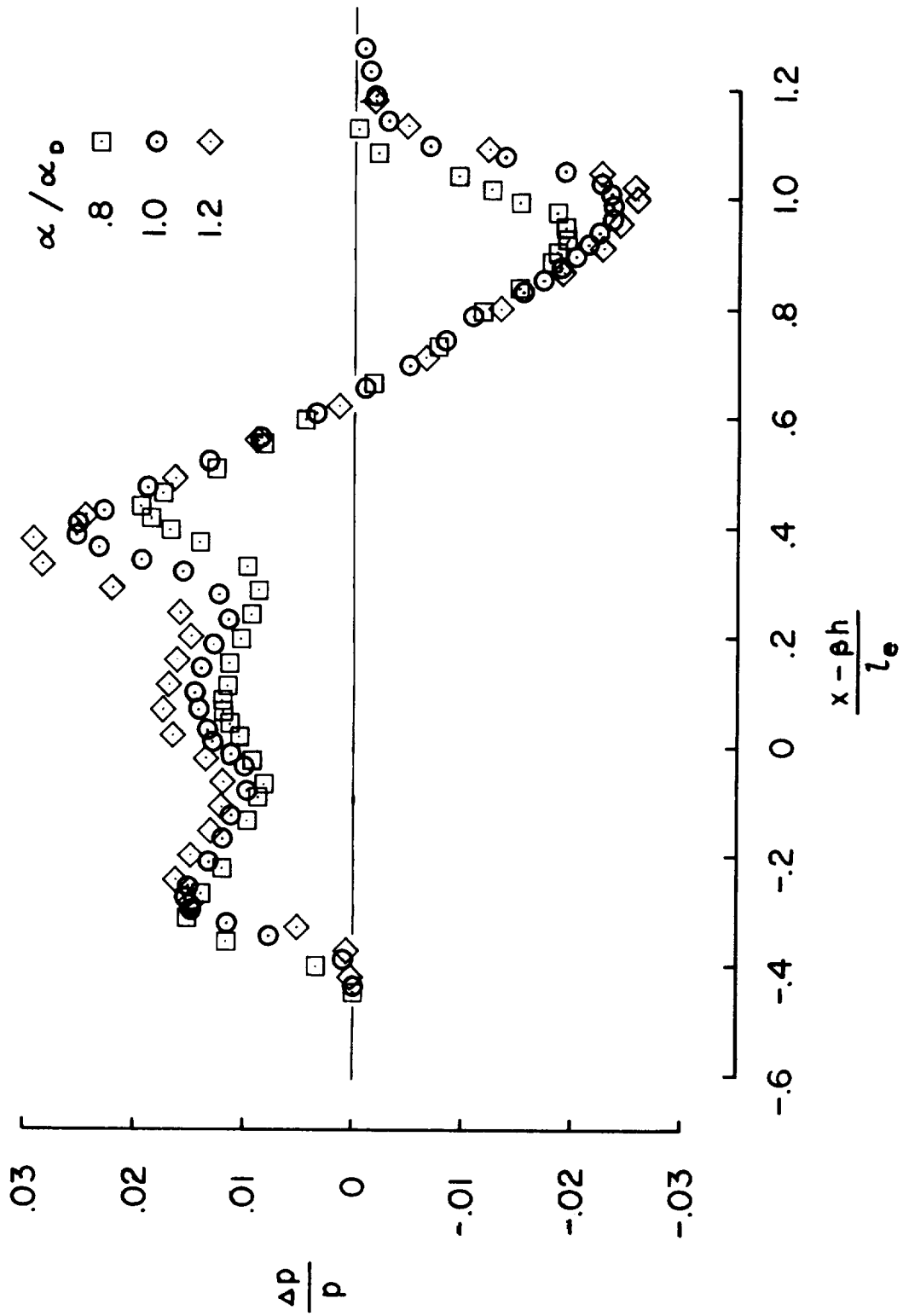
(d) Reference models and Mach 1.5 low-boom arrow-wing model.

Figure 12.- Concluded.



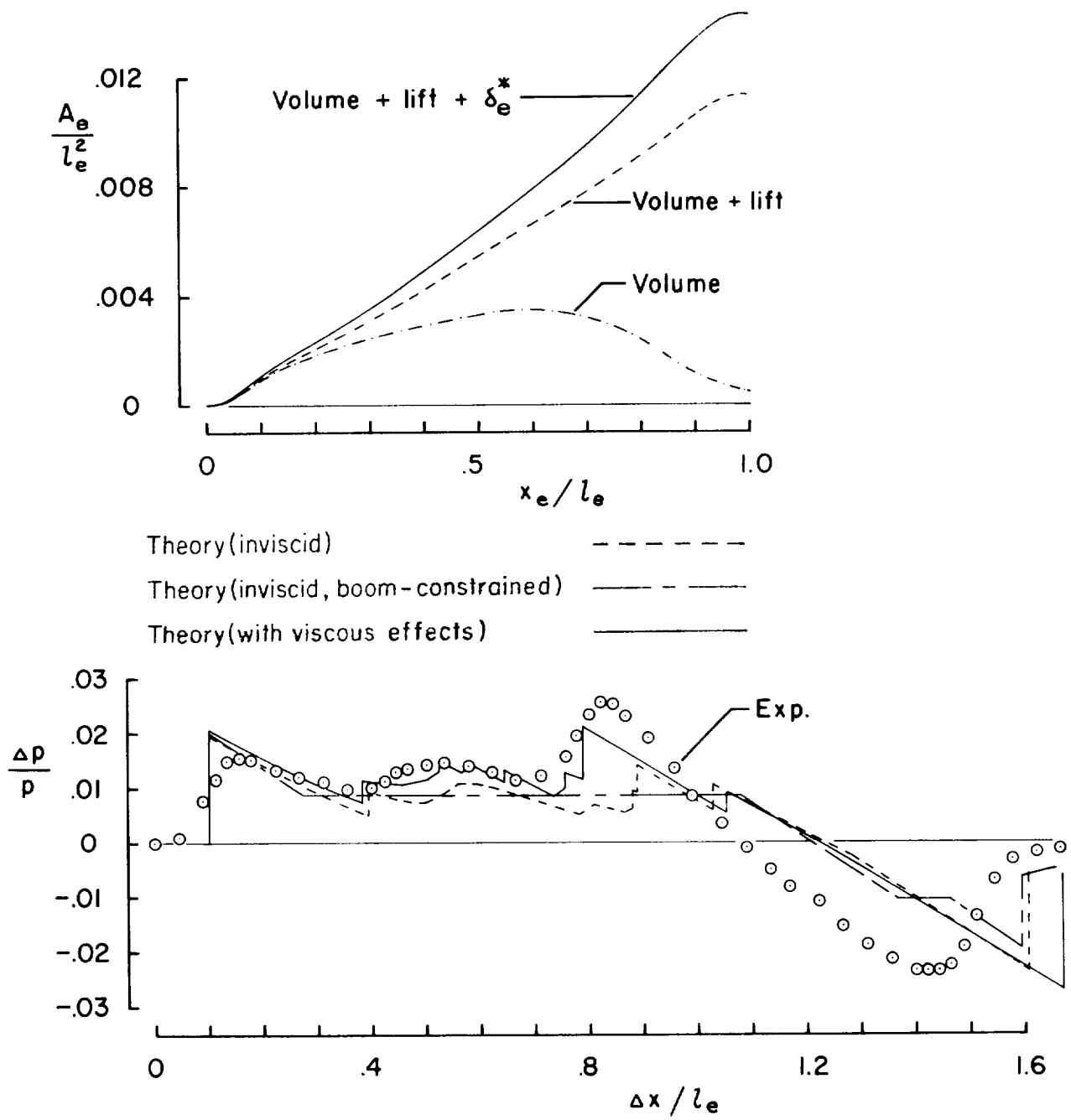
(a) $\alpha = \alpha_D$ with $M = 2.6, 2.7,$ and 2.8 .

Figure 13.- Measured pressure signature sensitivity with Mach number and angle of attack.
Mach 2.7 low-boom arrow-wing model.



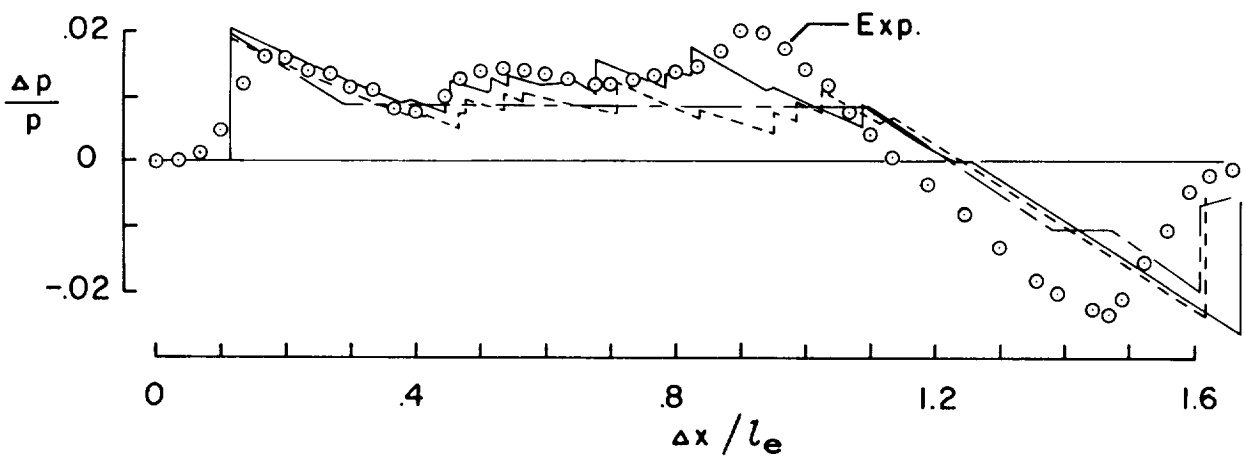
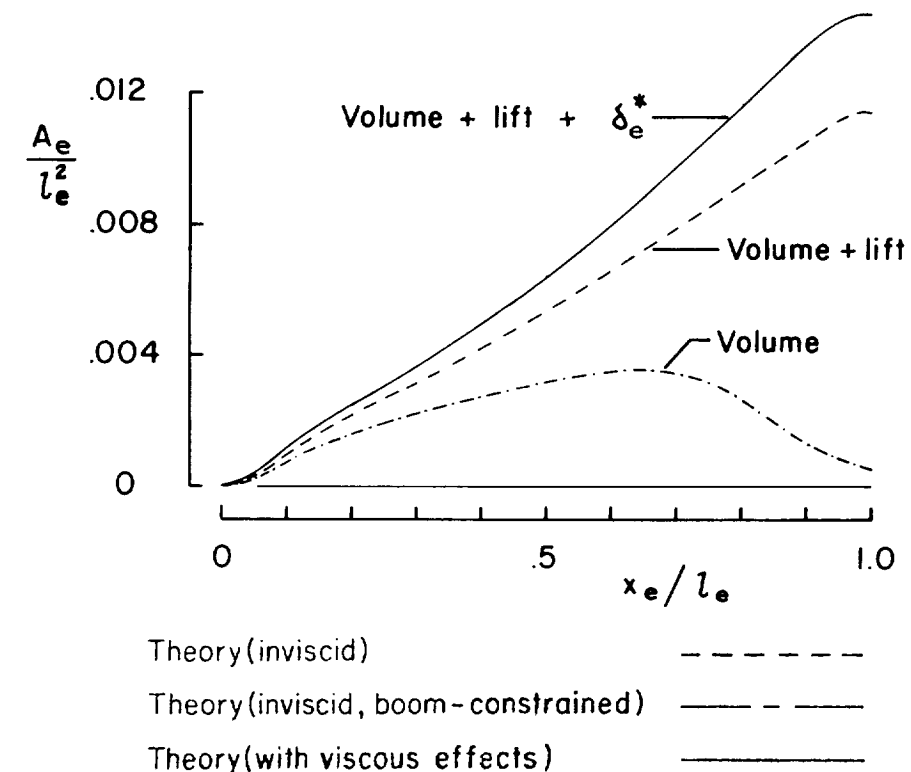
(b) $M = 2.7$ with $\alpha/\alpha_D = 0.8, 1.0, \text{ and } 1.2.$

Figure 13.- Concluded.



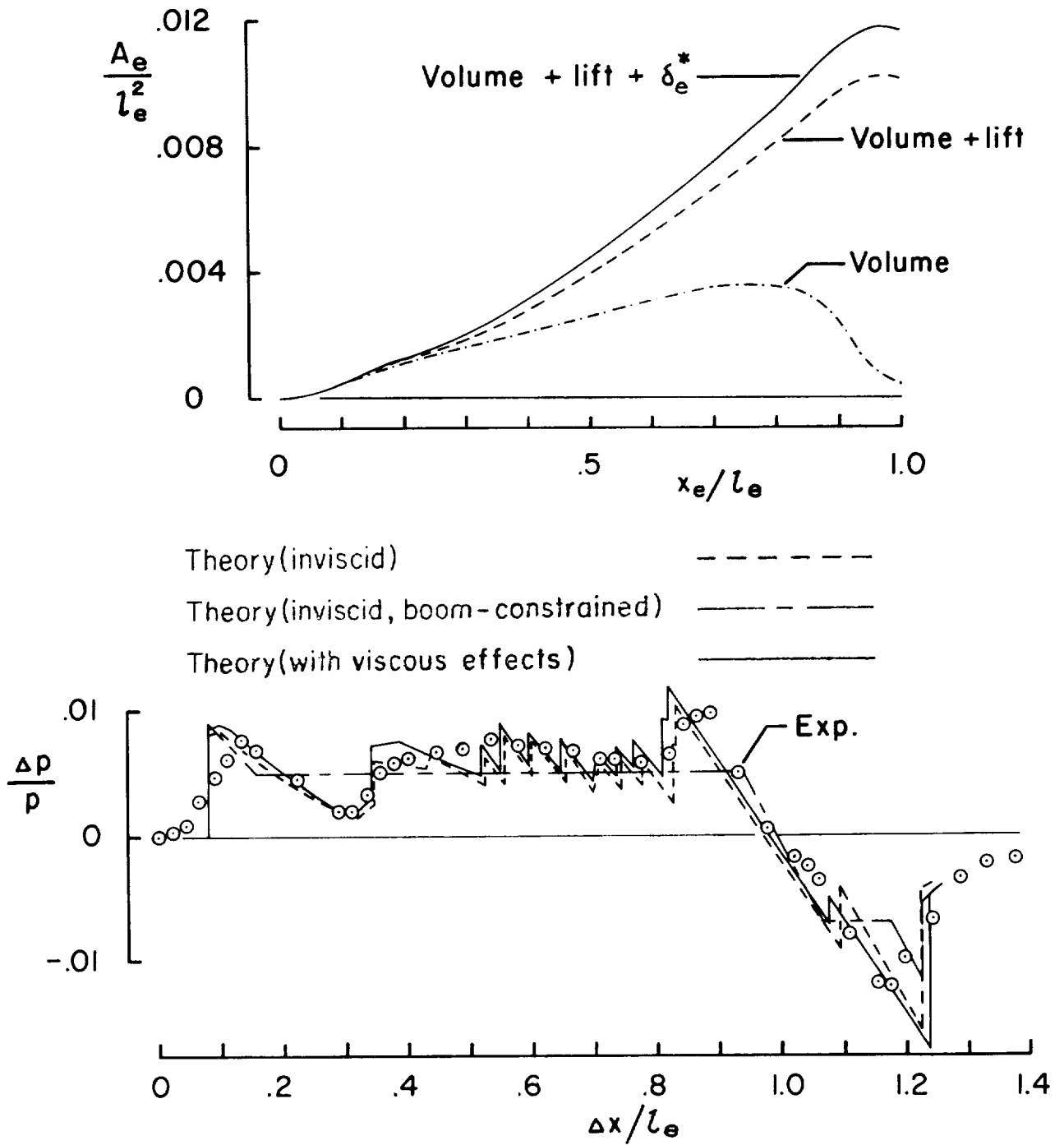
(a) Mach 2.7 low-boom arrow-wing model.

Figure 14.- Comparison of theory and experiment at M_D , $h/l_e = 3$, and $\alpha/\alpha_D = 1.0$.



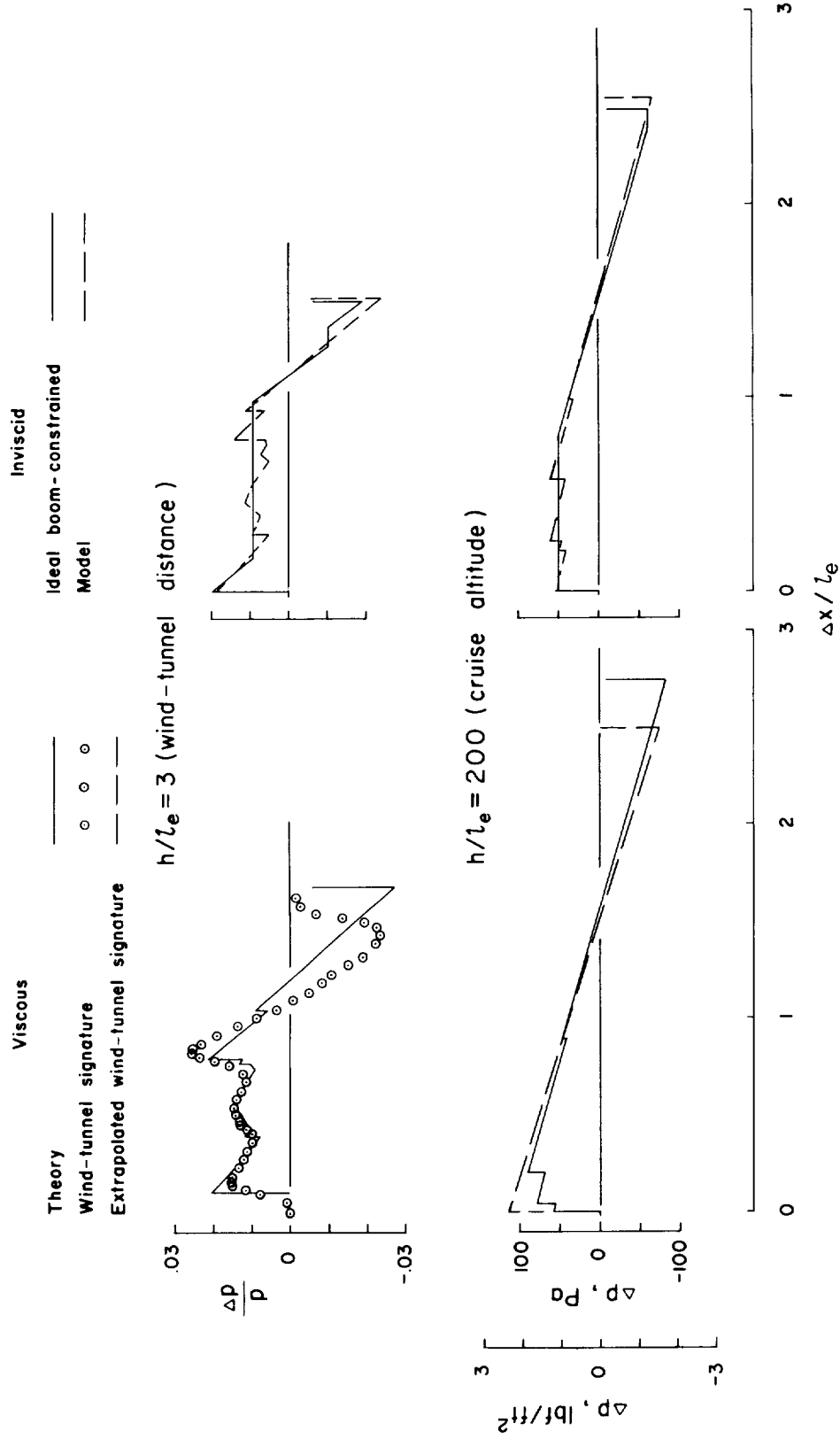
(b) Mach 2.7 blunted arrow-wing model.

Figure 14.- Continued.



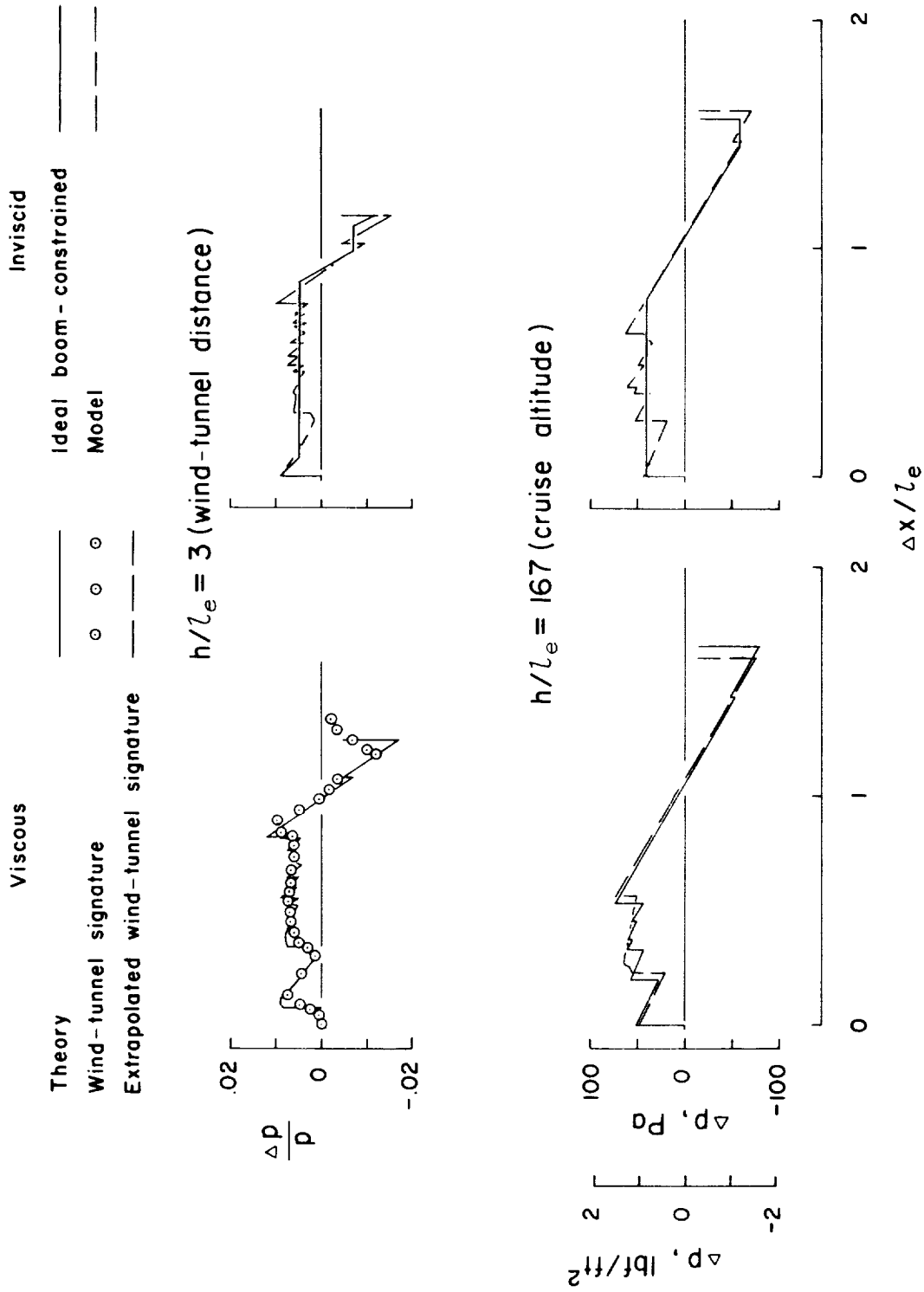
(c) Mach 1.5 low-boom arrow-wing model.

Figure 14.- Concluded.



(a) Mach 2.7 low-boom arrow-wing model. $M = 2.7$; $\alpha/\alpha_D = 1.0$; $h = 18\,288\text{ m (60\,000 ft)}$; $K_r = 1.9$.

Figure 15.- Comparison of extrapolated signatures with and without boundary-layer effects.



(b) Mach 1.5 low-boom arrow-wing model. $M = 1.5$; $\alpha/\alpha_D = 1.0$; $h = 15\,240$ m (50 000 ft); $K_T = 1.9$.

Figure 15.- Concluded.



1. Report No. NASA TP-1421		2. Government Accession No.		3. Recipient's Catalog No.	
4. Title and Subtitle WIND-TUNNEL INVESTIGATION OF THE VALIDITY OF A SONIC-BOOM-MINIMIZATION CONCEPT				5. Report Date October 1979	
				6. Performing Organization Code	
7. Author(s) Robert J. Mack and Christine M. Darden				8. Performing Organization Report No. L-12661	
				10. Work Unit No. 517-53-43-03	
9. Performing Organization Name and Address NASA Langley Research Center Hampton, VA 23665				11. Contract or Grant No.	
				13. Type of Report and Period Covered Technical Paper	
12. Sponsoring Agency Name and Address National Aeronautics and Space Administration Washington, DC 20546				14. Sponsoring Agency Code	
15. Supplementary Notes					
16. Abstract A wind-tunnel investigation has been conducted to determine the validity of a sonic-boom-minimization theory. Five models - two reference and three low-boom constrained - were tested at design Mach numbers of 1.5 and 2.7. Results showed that the pressure signatures generated by the low-boom models had significantly lower overpressure levels than those produced by the reference models and that small changes in the Mach number and/or the lift caused relatively small changes in the signature shape and overpressure level. Boundary-layer effects were found to be sizable on the low-boom models, and when viscous corrections were included in the analysis, improved agreement between the predicted and the measured signatures was noted. Since this agreement was better at Mach 1.5 than at Mach 2.7, it was concluded that the minimization method was definitely valid at Mach 1.5 and was probably valid at Mach 2.7, with further work needed to resolve the uncertainty.					
17. Key Words (Suggested by Author(s)) Sonic boom Minimization theory Experimental study			18. Distribution Statement Unclassified - Unlimited Subject Category 02		
19. Security Classif. (of this report) Unclassified		20. Security Classif. (of this page) Unclassified		21. No. of Pages 44	22. Price* \$4.50

* For sale by the National Technical Information Service, Springfield, Virginia 22161